GEOLOGICA CARPATHICA, OCTOBER 2017, 68, 5, 479–500 doi: 10.1515/geoca-2017-0031

Tectono-sedimentary analysis using the anisotropy of magnetic susceptibility: a study of the terrestrial and freshwater Neogene of the Orava Basin

MACIEJ ŁOZIŃSKI✉, PIOTR ZIÓŁKOWSKI and ANNA WYSOCKA

University of Warsaw, Faculty of Geology, Żwirki i Wigury 93, 02-089 Warszawa, Poland; ✉maciej.lozinski@student.uw.edu.pl

(Manuscript received February 2, 2017; accepted in revised form June 9, 2017)

Abstract: The Orava Basin is an intramontane depression filled with presumably fine-grained sediments deposited in river, floodplain, swamp and lake settings. The basin infilling constitutes a crucial record of the neoalpine evolution of the Inner/Outer Carpathian boundary area since the Neogene, when the Jurassic–Paleogene basement became consolidated, uplifted and eroded. The combination of sedimentological and structural studies with anisotropy of magnetic susceptibility (AMS) measurements provided an effective tool for recognition of terrestrial environments and deformations of the basin infilling. The lithofacies-oriented sampling and statistical approach to the large dataset of AMS specimens were utilized to define 12 AMS facies based on anisotropy degree (P) and shape (T). The AMS facies allowed a distinction of sedimentary facies ambiguous for classical methods, especially floodplain and lacustrine sediments, as well as revealing their various vulnerabilities to tectonic modification of AMS. A spatial analysis of facies showed that tuffites along with lacustrine and swamp deposits were generally restricted to marginal and southern parts of the basin. Significant deformations were noticed at basin margins and within two intrabasinal tectonic zones, which indicated the tectonic activity of the Pieniny Klippen Belt after the Middle Miocene. The large southern area of the basin recorded consistent N-NE trending compression during basin inversion. This regional tectonic rearrangement resulted in a partial removal of the southernmost basin deposits and shaped the basin's present-day extent.

Keywords: Orava–Nowy Targ Basin, Neogene, intramontane basins, basin inversion, facies analysis, anisotropy of magnetic susceptibility.

Introduction

The anisotropy of magnetic susceptibility method has been approved for decades as an effective tool in a broad spectrum of geological applications (e.g., Graham 1954; Hrouda 1982; Tarling & Hrouda 1993; Parés 2015). Any rock composed of mineral grains is characterized by a magnetic susceptibility reflecting the minerals' contribution to an applied external magnetic field. This physical feature usually differs with respect to the direction of the field, which is referred to as the anisotropy of magnetic susceptibility (AMS). For paramagnetic and diamagnetic grains (such as clay minerals, quartz and carbonates) the AMS is a result of their specific magnetocrystalline anisotropy, whereas ferromagnetic grains (typically iron oxides and sulphides) may additionally have the easy direction of magnetization related to the shape and size of grains (Rees 1965), as well as to intergranular interactions. The AMS measurement reflects the total effect of all grains in a specimen and is predominantly studied in a phenomenological and descriptive way. The result depicts a sediment or rock preferred grain alignment and is usually interpreted in terms of bedding orientation and flow directions, as well as structural lineation and foliation being a result of deformation (see discussion in Hrouda 1982).

The application of the AMS method in orogeny-related basins and accretionary prisms predominantly concerns a structural interpretation of strain directions (e.g., Hrouda & Potfaj 1993; Parés et al. 1999; Kanamatsu & Herrero-Bervera 2006; Hrouda et al. 2009; Mazzoli et al. 2012) and turbidity current directions (e.g., Tamaki et al. 2015), while hemipelagic and pelagic sediments are examined for the occurrence and directions of bottom currents (e.g., Ellwood & Ledbetter 1977; Shor et al. 1984; Joseph et al. 1998; Park et al. 2000; Baas et al. 2007; Parés et al. 2007). The sedimentological analysis supported by AMS measurements has also been done in a variety of sedimentary settings, namely: deep sea fans and turbidity deposits (von Rad 1970), deep-sea mass transport deposits (Novak et al. 2014), alluvial fine-grained sediments (Garcés et al. 1996; Park et al. 2013), pyroclastic density currents and lahar deposits (Biró et al. 2015; Ort et al. 2015), as well as glacial sediments (Eyles et al. 1987; Gravenor & Wong 1987). In this study we aim to analyse fine-grained freshwater and terrestrial deposits of the Orava Basin (Łoziński et al. 2015) focusing on both sedimentary and structural aspects of the AMS results.

The Orava Basin is a Neogene intramontane basin in the Western Carpathians. The time of the basin's development corresponds to the termination of formation of the Outer

Carpathians thrust-and-fold belt, and submission of the orogeny to exposure and erosion (e.g., Jankowski & Margielewski 2014). The Orava Basin comprises the excellent sedimentary record of the structural and environmental evolution of the studied region of that time. This involves the transition from marine to terrestrial sedimentation (Birkenmajer 1954; Cieszkowski 1995), development of regional strike-slip movements in the Carpathians (Kováč et al. 1993) and the uplift and erosion of individual blocks of predominantly Paleogene rocks in the vicinity of the basin (Tokarski et al. 2012; Jankowski & Margielewski 2014). However, fine-grained deposits often are macroscopically structureless and since they lack correlation indicators, they are not easy to interpret. We expect that the application of the AMS method may significantly contribute to knowledge of the basin's history.

This study is based on the very detailed facies study of lacustrine, flood plain, alluvial, and swamp settings presented in Łoziński et al. (2015). The local facies model for the well-exposed section of the Oravica River has been verified and adapted in this paper to describe facies within the whole basin. The problem of the interplay of tectonic and sedimentary factors in determining the AMS fabrics for the moderately deformed Oravica River section has already been discussed in a case-study paper of Łoziński et al. (2016). The considerable variety of the obtained AMS fabrics suggested a possible recognition of the AMS facies reflecting the depositional processes. The aim of this paper is to construct a model for fine-clastic deposits of the Orava Basin, which hopefully will be for universal use as well. This study is based on a large data set of field-collected spatially oriented AMS specimens (1930 specimens from 85 locations, see Appendix) collected with respect to the recognized lithofacies. The AMS results are interpreted to reconstruct the facial scheme of the basin and to depict its deformational style and possible tectonic strain directions.

Geological setting

The Orava Basin is currently an approximately 35 km long and 15 km wide intramontane depression straddling the Inner/Outer Carpathian border (Fig. 1). It is filled with predominantly terrestrial clastic sediments which overlie preconsolidated, folded and partially eroded older units: mostly the Magura Nappe, Pieniny Klippen Belt, and Podhale Synclinorium. The northernmost unit, Magura Nappe, is built up of Albian/Cenomanian–Miocene sandstones, mudstones, and marls (Birkenmajer & Oszczypko 1989; Cieszkowski et al. 1989; Cieszkowski 1995; Malata et al. 1996). The Pieniny Klippen Belt comprises strongly deformed Early Jurassic–Paleogene limestones, marls, mudstones, calcarenites, and conglomerates (e.g., Birkenmajer 1960). The southernmost part of the Orava Basin in underlain by the Podhale Synclinorium, a folded Lutetian/Bartonian to Egerian part of the Central Carpathian Paleogene Basin (Gross et al. 1993b; Olszewska & Wieczorek 1998; Soták 1998a,b; Garecka 2005). After these units underwent folding and erosion, the W–E-trending elongated depression was formed. The onset time of the deposition in the Orava Basin is poorly constrained, ranging from Late Oligocene (Woźny 1976), through Badenian

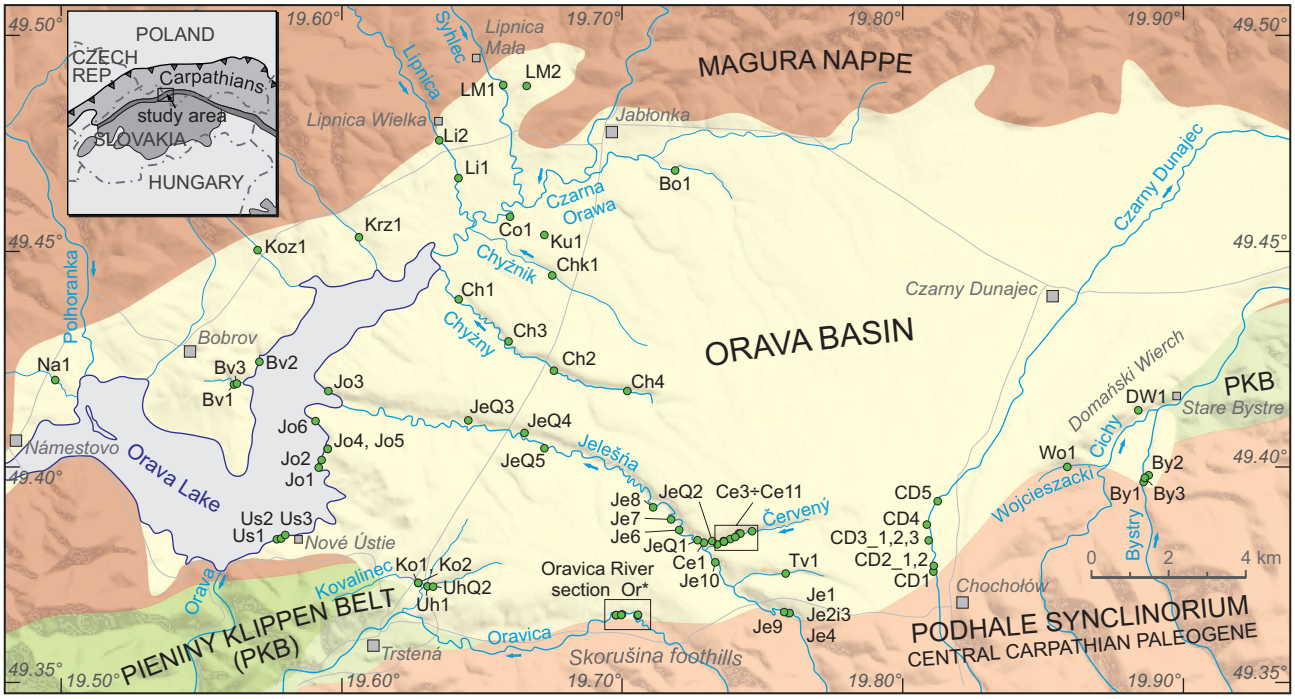

Fig. 1. The simplified geological map of the Orava Basin and its vicinity. The AMS sampling locations are marked with dots and sample names. For detailed locations of the Oravica River section samples see Łoziński et al. (2016).

(Oszast & Stuchlik 1977), Late Badenian or Sarmatian (Cieszkowski 1995), to Sarmatian (Nagy et al. 1996). However, most authors agree about the Middle Miocene age of the basin's origin which is based on the widely-studied flora associations, and corresponds well with the opening time of the transtensional basins inside the Carpathian orogenic belt (Kováč et al. 1993). The dominant siliciclastic basin infill has been probably derived from older eroded units exposed in the vicinity of the basin (Birkenmajer 1954; Watycha 1976a; Tokarski et al. 2012). The deposition of conglomerates, sandstones, clayey siltstones, claystones, and coals took place in terrestrial and freshwater environments: alluvial fans, rivers, flood plains, lakes and swamps (Watycha 1976a; Birkenmajer 1978; Kukulak 1998; Łoziński et al. 2015). The sedimentary bodies of deposits are laterally and vertically restricted, and strongly depend on their paleotopographic position. According to Birkenmajer (1954) and Watycha (1976a), alluvial fans with coarse clastics have been developed within the basin margins. Grain size decreased towards the centre of the basin, where river-associated and stagnant-water deposition took place within extensive floodplains and swampy areas. The abundant plant vegetation within the wet areas favoured preservation of organic matter and initiated brown coal formation (e.g., Polášek 1959; Oszast & Stuchlik 1977; Kołcon & Wagner 1991). Lacustrine deposits represent episodic lakes and no basin-scale reservoir has been recorded during the basin's evolution (Watycha 1976a; Łoziński et al. 2015). The sedimentary environment could have been disrupted by volcanic ashfall events resulting in tuffite deposition (Beleš 1974; Sikora & Wieser 1974; Kołcon & Wagner 1991; Łoziński et al. 2015). The topmost deposits of the Quaternary age (Watycha 1976a; Baumgart-Kotarba et al. 1996) lie often discordantly above older deposits. Apart from fine clastics, they also represent large alluvial fans with pebbles and cobbles derived from adjacent areas and the Tatra Mts. This records a major Quaternary uplift of adjacent source areas and marginal parts of the basin, which could have had a wider extent in the Neogene (Tokarski et al. 2012; Łoziński et al. 2015). The depression could have been formed as a pull-apart basin (e.g., Pospíšil 1990; Baumgart-Kotarba 2001), a releasing-bend structure along the Pieniny Klippen Belt (Pomianowski 2003), or as a series of tectonic subbasins within the flexure of the Outer Carpathian arc (Struska 2008).

Methods

This study is based on field sedimentological and tectonic observations, magnetic measurements on a set of specimens collected from outcrops, and pre-existing geological data: detailed geological maps (Watycha 1976b, 1977a,b,c; Gross et al. 1993a) and documentation of boreholes Czarny Dunajec-IG1 (Watycha 1971) and OH-1 (Pulec 1976). Field observations included: all macroscopic sedimentary and diagenetic structures, grain size, colour, level of consolidation, presence of tectonic fractures, faults and ductile deformation, bedding orientation, as well as position in present-day sedimentary environment with special attention to mass movements. The age of the studied deposits considered to be Neogene in this paper could not be exactly determined. Instead, the sedimentological criterion has been used: all fine-clastic sediments which could not be deposited in a present-day sedimentary environment have been taken into account.

The sampling process for magnetic measurements was intended to give a 25-specimen representation of a sediment mass of a specific lithofacies found in a studied location, what is referred to here as a "lithofacies-oriented sampling". The conventional method of sampling a sedimentary vertical sequence has been generally neglected here, since a sedimentary environment in terrestrial settings may change within small distances laterally and vertically. The sampling was conducted using brass samplers hit with a rubber hammer into a fresh surface of deposits (see the equipment in Łoziński et al. 2016). A cylinder obtained from a sampler has been cut into standard ø25.4 mm-wide and 22 mm-tall magnetic specimens. All specimens have been collected with measured azimuth, dipping angle and (in most cases) the axial rotation angle of the sampler. It should be noted that weakly consolidated deposits could have been altered by the hitting force and acquired a false tectonic fabric. This has been examined by applying different sampling azimuths, and then testing the correlation between sampling direction and the AMS ellipsoid directions. The total specimen dataset includes 1930 specimens (322 specimens have been reused from Łoziński et al. 2015; names with prefix Or-) grouped into 85 statistical samples representing various lithofacies and localities (Fig. 1).

The specimens collected have been measured for volume bulk magnetic susceptibility and its anisotropy at field intensity 200 A/m and frequency 976 Hz using a MFK1-FA kappabridge with a 3D rotator (AGICO, Czech Republic). The AMS obtained during measurements is defined as a second-rank tensor with symmetrical 3×3 matrix representation. The analysis of AMS is performed using convenient anisotropy parameters: main axes of anisotropy ellipsoid k1, k2, and k3 (axis of maximum, intermediate, and minimum susceptibility accordingly), anisotropy degree P=k1/k3, lineation L=k1/k2, foliation F=k2/k3, and anisotropy shape $T = [2\log(k2)-\log(k1)-\log(k3)] / [\log(k1)-\log(k3)]$ (Hrouda 1982 and references therein). Multispecimen statistical processing has been done according to mean tensor calculation defined in Jelínek & Kropáček (1978).

The magnetic mineralogy was assessed by two methods: the Lowrie test and thermoanalysis, in which the distinctive, characteristic coercivities and thermomagnetic properties of the common ferromagnetic minerals have been used. The analysis of the acquisition curve of isothermal remanent magnetization (IRM) combined with subsequent thermal demagnetization of the IRM provided the interpretation of the ferromagnetic mineral content of a rock (Lowrie 1990). The 20 specimens were given an isothermal remanence (IRM), in steps from 0.014 T up to 3 T along Z-axis, using

magnetization in a pulse magnetizer MMPM10 (Magnetic Measurements, Great Britain). After each step the IRM was measured using a spinner magnetometer JR6A (Agico). Afterwards, different coercivity fractions of IRM were remagnetized in successively smaller fields along two orthogonal directions: 0.4 T along the Y-axis and 0.12 T along the X-axis. After thermal demagnetization of 8 representative specimens in a MMTD80A furnace (Magnetic Measurements), each orthogonal component of the composite IRM was plotted separately. These results were supplemented by thermoanalysis by measuring bulk susceptibility of 3 specimens during heating up to 700 °C and cooling down in a KLY3S/CS3 kappabridge (Agico). All magnetic procedures were carried out at the European Centre for Geological Education (Chęciny, Poland), except for the thermoanalysis which was carried out at the Institute of Geophysics, Polish Academy of Sciences (Warsaw, Poland). The data was acquired using SAFYR6, REMA6 and SUSTE7 programs (Agico) and processed with an R statistical software (R Core Team 2015).

Results

Facies model

The sedimentological analysis of this study is based on the classical concept of lithofacies and facies associations (see summary in Miall 2000). This practical approach aims at defining sedimentary units based on macroscopic sediment description and interpreting them in terms of physical conditions, e.g.: mechanism of sediment transport, current velocity, settling process, and biogenic activity. The analysis of lithofacies associations in vertical and lateral extent is a basis for interpretation of sedimentary environments. This kind of analysis has already been applied to the 90-m thick diversified section of the Oravica River in the southern part of the Orava Basin in Łoziński et al. (2015). For the purpose of this study a new lithofacies scheme has been constructed for the whole Orava Basin (Table 1).

The matrix-supported breccia (Gmm) is composed of angular clasts of older units spread in a predominantly muddy matrix and lacking any sedimentary structures (Fig. 2). It has been interpreted as a plastic debris-flow deposit which was confined to areas of considerable terrain relief, probably during pre-basinal basement erosion and later, at basin margins. In turn, the clast-supported conglomerate (Gcm, Fig. 3A) represents deposits of low sediment concentration flow within alluvial fans having a large lateral extent. Lithofacies Gh, Sh Sp, and St depict bedforms deposited in a water current of different strength and flow regimes usually within a fluvial channel. Lithofacies Sm occurs typically as a structureless intercalation within clayey and silty lithofacies CL, Fl, and Fm (Fig. 2).

The massive clayey siltstone (lithofacies Fm, Fmc, and Fmm) may reach thickness of several metres, and typically lacks any sedimentary structures. Similar massive lithofacies with rhizoliths may be found within present-day river banks (Fig. 3B), usually overlying alluvial conglomerates (lithofacies Gh). Fresh non-consolidated muds are well-oxidized and often rich in organic matter, which makes them convenient for biogenic activity. Faunal bioturbation is followed by a quickly developing plant vegetation resulting in root bioturbation. Additionally, deposited muds being within a vadic zone, undergo multiple changes in relative humidity. This process has been recognized to degrade original sedimentary structure into massive structure due to particle movements during shrinkage and swelling (Wetzel & Einsele 1991). The observable stage of biogenic activity is exhibited by a sublithofacies Fmm (Fig. 3C) being in most cases a relatively young deposit of the Orava Basin. This subdivision of lithofacies Fm is defined by its weak consolidation, significant porosity, and abundant root moulds and tubules (Klappa 1980) emphasized by red oxidation zones. However, these features may also be achieved by weathering and reworking of older exhumed deposits. The lithofacies Fm (Fig. 3D) represents compacted overbank deposit which gained its massive structure shortly after sedimentation. It lost its biogenic porosity and gained a typical monotonous bluish-grey colour in oxygen-deficient conditions after burial. This lithofacies in an outcrop often exhibits muddy clasts (Fig. 3D) which are known to be formed on weathered surfaces during repetitive drying-wetting cycles (Wetzel & Einsele 1991). Rare rhizoliths are present in forms of carbonate rhizocretion horizons, as well as root tubules and petrified root tissues preserved within siderite concretions (Bojanowski et al. 2016). The presence of siderite concentrations and siderite cemented horizons defines a sublithofacies Fmc (Fig. 3E) and is interpreted as a result of anoxic diagenetic condition and bacterial methanogenesis under a swamp.

The heterolithic sandstone-dominated lithofacies Hs comprises an association of sandstone, siltstone and claystone layers. Grain size usually exhibits gradual change. In some cases the cyclicity is poorly defined, but the regular Bouma cycles (Tb–Te) may be present as well. The latter structure predestines this lithofacies to be interpreted as a low-density turbidity current deposit. However, in general this lithofacies may occur in various settings where current flow is ephemeral. Heterolithic siltstone-dominated deposits (lithofacies Hf, Fig. 3F) show very subtle laminations and rare ripple cross-beddings. The erosive capability of the environment must have been very restricted, and the flow deposition alternated with a long time of stagnant water settling. Hence, the distal low-density turbidity current seems the most adequate interpretation. Lithofacies Fl and CL represent mostly deposition from suspension. Laminated siltstones (lithofacies Fl, Figs. 2, 3G) usually reveal well parting along bedding planes. This is in contrast to typically massive claystones (CL) where bedding is distinct only due to the admixture of plant detritus. The organic matter content varies ranging gradually from grey pure claystones (CL), through black coaly claystones (CCL) to pure coals (C) (Fig. 3H). The rare freshwater limestone beds (lithofacies L) usually accompany coal seams. The volcanic

Table 1: Lithofacies distinguished on the basis of their macroscopic features. Based on Miall (2006) classification, the results of this study, and: Sikora & Wieser 1974 [1], Kołcon & Wagner 1991 [2], Tokarski et al. 2012 [3], Łoziński et al. 2015 [4] and Bojanowski et al. 2016 [5].

Facial code	Lithofacies	Description and interpretation	Interpretation
L	freshwater limestone	beds up to 30 cm thick; calcitic rock; well-preserved mollusc shells; white, yellow; [4]	authigenic calcite precipitation
T	tuffite	beds from a few millimetres to 2 m thick; pyroclastic silty and clayey deposit with admixture of terrigenous fine clastic sediments; massive or laminated, rarely cross-bedded; white, yellow; green when wet; [1] [2] [4]	ashfall deposition, may be altered by current
C	coal	beds typically up to 40 cm thick; lignites from unlithified plant detritus to shiny and brittle rock; brown to black; [2] [4]	phytogenic accumulation
CCL	coaly claystone	beds typically up to 20 cm thick; claystone abundant in organic matter; brown to black; [4]	phytogenic accumulation with influx of siliciclastic material
CL	claystone	beds up to 50 cm; massive structure to weak lamination; subordinately plant detritus admixture; dark grey, grey or grey-blue; [4]	suspension fallout deposition
Fl	laminated or massive clayey siltstone	varied thicknesses; subtle laminations or massive structure with weak tendency to break along bedding surfaces; grey to dark grey; [4]	suspension fallout, may be current-driven
Hf	siltstone-dominated heterolithic deposits	varied thicknesses; normally graded siltstones and claystones; laminated with subordinate ripple cross-bedding; grey to dark grey; [4]	low-density turbidity currents or ephemeral ripple bed transport
Hs	sandstone-dominated heterolithic deposits	varied thicknesses; normally graded sandstones, siltstones and rare claystones; laminated or ripple cross-bedded; occasionally Tb-e Bouma sequences; grey, dark grey or grey-blue; [4]	low-density turbidity currents or ephemeral ripple- and plane- bed transport
Fm	massive clayey siltstone	varied thicknesses (up to several meters); siltstone and clayey siltstone; predominantly massive structure, very rare indistinct laminations; locally calcitic concretions; rare muddy clasts (up to 15 cm) appearing at weathered surface; grey-blue or red; [4]	mud-suspension fallout, may be current-driven; original structure overprinted by bioturbation and/or synsedimentary weathering
Fmc	massive clayey siltstone with siderite concretions	lithofacies Fm with siderite concentrations, concretions and horizons; grey-blue or red; [4] [5]	lithofacies Fm influenced by geo-chemical processes related to soil or swamp development
Fmm	massive clayey siltstone and sandstone (mottled)	lithofacies Fm; often sandy; locally single pebbles; weakly consolidated; grey with orange to red spots around pores of biogenic origin (rhizoliths, Fig. 3B and C)	lithofacies Fm at an initial stage of diagenesis, altered by young biogenic activity
Sm	massive sandstone	varied thicknesses; usually clayey and silty; fine- and medium- grained; grey or grey-blue;	grain flow, rapid deposition
Sh	horizontally laminated sandstone	fine- and medium- grained; often abundant plant detritus; rarely muddy intraclasts; grey, red to brown; [4]	plane-bed flow
Sp, St	planar and trough cross-bedded sandstone	beds up to 1 m; usually clayey and silty; fine- to coarse- grained; common plant detritus; rare muddy intraclasts; grey, red to brown; [4]	2D and 3D bedforms (dunes)
Gh	horizontally bedded and imbricated conglomerates	up to 50 cm thick beds and lenses; indistinct horizontal bedding and imbrication, often massive; predominantly composed of monomict clasts: sandstones, mudstones, subordinately limestones, quartzites, crystalline rocks and others; grey, red to brown; [3]	bedload sheets, lag deposits
Gcm	clast-supported monomict conglomerate	several meters thick; massive; predominantly composed of monomict clasts: sandstones, mudstones, subordinately limestones, quartzites, crystalline rocks and others; small amount of sandy or muddy matrix; grey, red to brown; [3] [4]	low sediment concentration flow
Gmm	matrix-supported breccia	several meters thick; breccia composed of monomict clasts: sandstones and mudstones, subordinately limestones; sandy and muddy matrix; grey, grey-blue [4]	cohesive debris flow

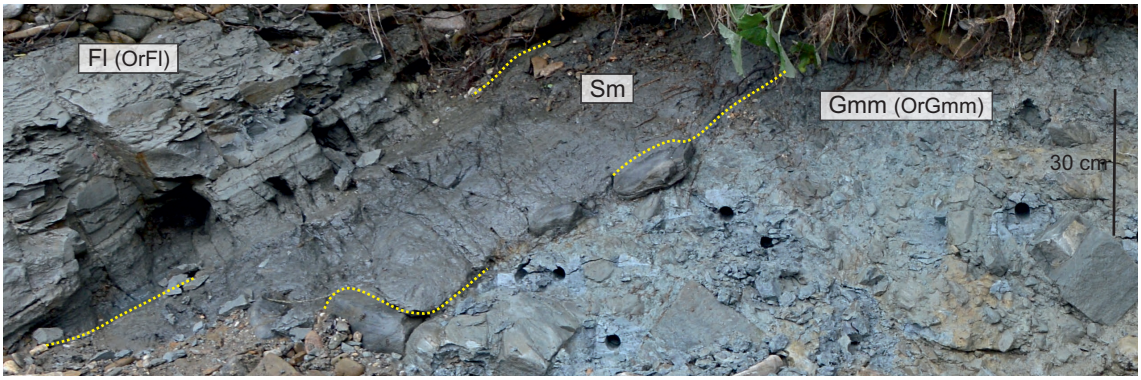

Fig. 2. Fine clastic lithofacies: massive sandstones (Sm) and laminated siltstones (Fl) overlie with sedimentary contact disorganized breccia (lithofacies Gmm) of inferred debris-flow origin (Oravica river, for detailed locations see Łoziński et al. 2016). AMS sample names are shown in brackets.

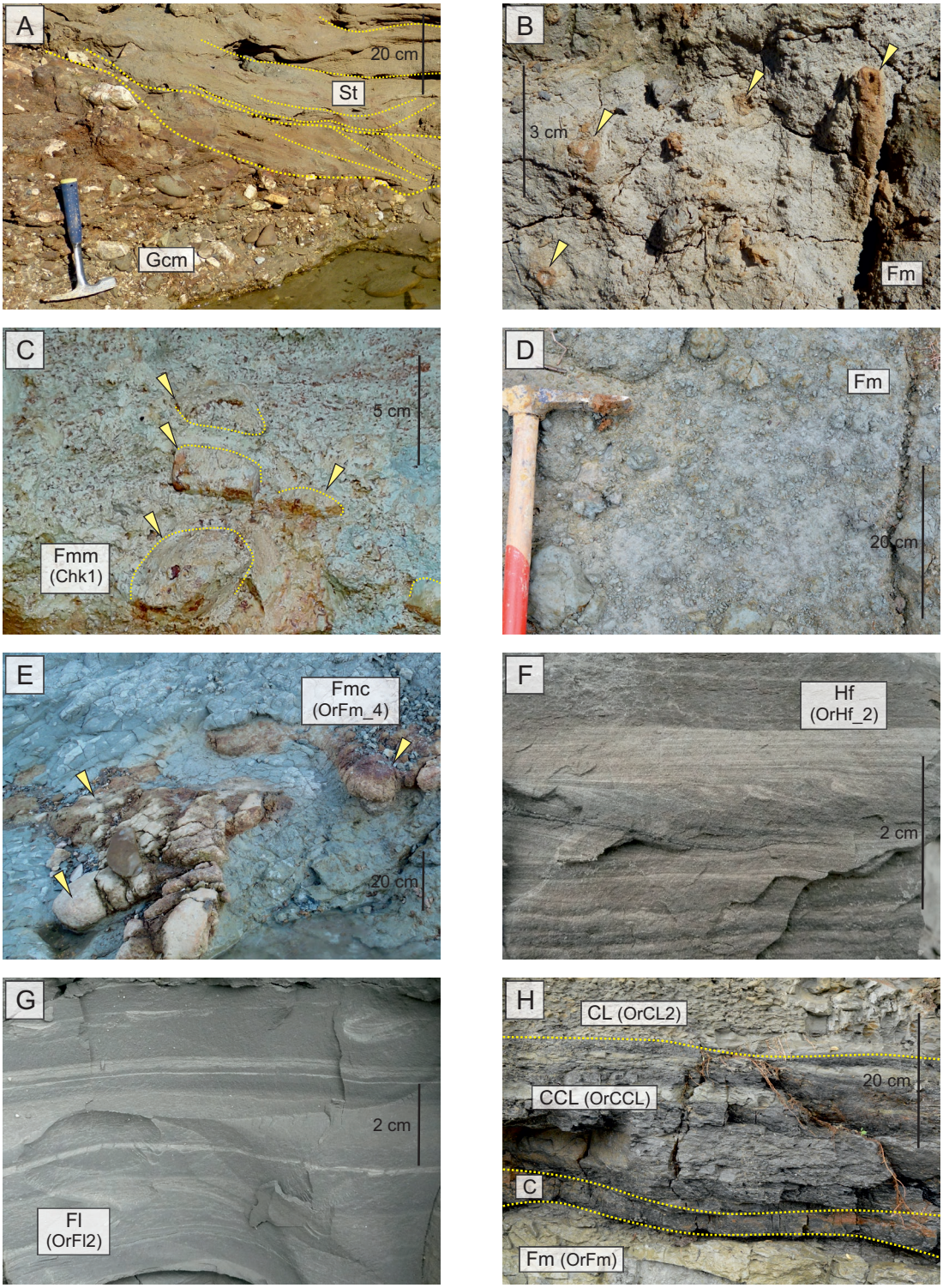

Fig. 3. Neogene lithofacies and sedimentary structures of fine clastics of the Orava Basin. AMS sample names are shown in brackets. **A** — River channel lithofacies: conglomerate (Gcm) consisting of sandstones, mudstones and limestones overlaid by trough cross-bedded sandstones (St) (Bystry stream). **B** — Present-day root cementation (marks) as an example of root bioturbation and quick decomposition of organic matter (floodplain terrace of Cichy stream). **C** — Single sandstone clasts (marks) in massive clayey siltstone (lithofacies Fmm – Chyżnik stream) with a specific mottled (grey with red spots) colour. **D** — Massive clayey siltstone (lithofacies Fm) exhibiting muddy clasts (weathering) on a wave-eroded surface (Orava Lake shore). **E** — Bluish floodplain massive clayey siltstone with red to brown siderite-cemented horizon (marks; lithofacies Fmc – Oravica river). **F** — Lacustrine siltstone-dominated heterolithic deposit with lamination and ripple cross-bedding (lithofacies Hf – Oravica river). **G** — Lacustrine claystones and laminated siltstones with a load-cast structure (lithofacies Fl – Oravica river). **H** — Floodplain clayey siltstone (lithofacies Fm) overlaid by swamp lithofacies association: coal (C), coaly claystone (CCL) and claystone (CL) exhibiting a gradual change in deposition (Oravica river, for detailed locations see Łoziński et al. 2016).

activity is recorded by tuffite layers and small intercalations (lithofacies T), usually strongly chemically weathered.

Levels of structural deformation

In order to regard the various levels of deformation in the AMS analysis, four levels of structural deformations have been introduced based on field observations. The *weakly consolidated* category denotes soft deposits lying horizontally, often mottled and porous due to young bioturbation, and lacking any tectonic features. The *consolidated* category does not have macroscopic pores, and is relatively better compacted than the first one. These two types prevail in the central part of the basin. Within the *moderately deformed* category, an irregular (or mostly one-directional) sets of joints, as well as normal faults, have been observed (Tokarski & Zuchiewicz 1998; Kukulak 1999; Łoziński et al. 2015). The moderately deformed strata are tilted typically from 5 to 30° and are exposed predominantly along the southern and south-eastern margin of the basin (from Nové Ústie to Stare Bystre village) and in the north (near Lipnica Mała and Lipnica Wielka villages). The *strongly deformed* category is used for deposits tilted strongly (50–90°) and/or revealing ductile deformation. Such a strong deformation has been observed or suggested by the AMS results near the Nové Ústie and Bobrov villages, as well as the Kovalinec, Červený, and Wojcieszacki streams.

Magnetic susceptibility carriers

According to the grain size analysis from the OH-1 borehole (Pulec 1976), clay- and silt-sized particles usually dominate, and sand grains are a minor admixture (typically 1÷15 %) except for sandy intercalations. Sand grains are mainly composed of quartz, pyrite, Fe-carbonates, limonite, apatite, chlorite, garnet, calcite, and muscovite. Ferromagnetic minerals are rare, but their content may be significant for magnetic measurements (typically: magnetite 0÷2 % of sandy grains), especially within Pliocene sediments (up to 7.5 % of sandy grains have been noticed). Clay minerals comprising 25–55 % of sediment mass are composed of beidellite, chlorite, illite and locally subordinate kaolinite (Wiewióra & Wyrwicki 1980; Łoziński et al. 2016). Around 95 % of the specimens measured in this study have a susceptibility of less than 500×10^{-6} SI. Considering the above, paramagnetic minerals (clay minerals) are expected to control the measured magnetic susceptibility in most cases.

In order to examine magnetic minerals, 8 representative specimens were chosen from 20 magnetically saturated specimens, which represented various sedimentary environments (Fig. 4A). The curve of the magnetic susceptibility vs. temperature (Fig. 4B; see Hrouda et al. 1997; Hrouda 2010) confirmed that the dominant component in low-susceptibility specimen 1 was paramagnetic (78–88 % of susceptibility inferred from hyperbola fitting), whereas high-susceptibility specimens 3 and 21 were controlled by ferromagnetic component. The results of magnetic saturation (Fig. 4A) showed that the majority of specimens saturated rapidly in fields up to 0.3 T, except for specimens 1 and 6, which saturated in the range of 1.5 to 2 T. The demagnetization curves obtained in the Lowrie test (Fig. 5; Lowrie 1990) showed that the magnetization values for these two specimens were dozens of times lower, and blocking temperatures of both fractions (soft

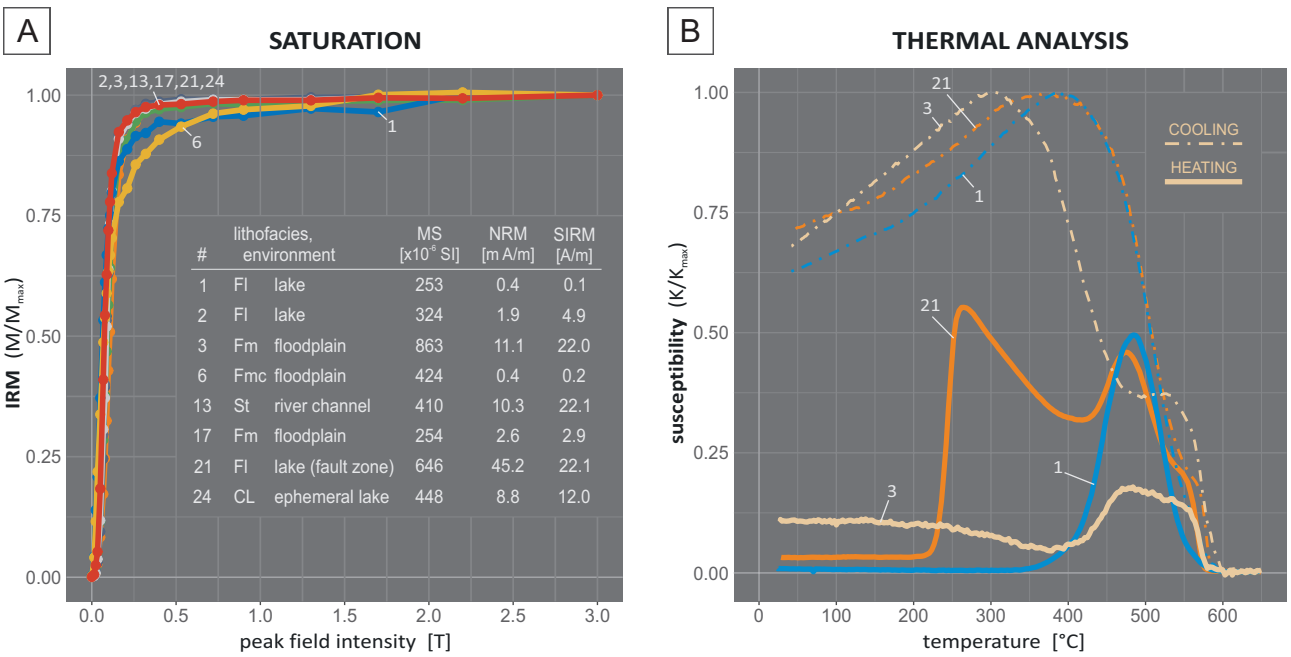

Fig. 4. Magnetic surveys of selected eight specimens from various depositional settings (table). **A** — The progressive acquisition of isothermal remnant magnetization (IRM). **B** — Variation of bulk susceptibility during heating and cooling.

575 °C and hard over 650 °C) were higher than for the others. The remaining specimens (2, 3, 13, 17, 21, 24) were almost completely demagnetized at a temperature of approx. 375 °C (soft fraction) and around 320–375 °C (medium and hard fraction). Complete demagnetization was reached at the temperatures similar to those of specimens 1 and 6. All this indicates a constant low content of magnetite in all tested specimens. In specimens 1 and 6 magnetite is the essential ferromagnetic mineral. In the other specimens, where the saturation magnetization is relatively high, the main ferromagnetic minerals *s.l.* are greigite (see Babinszki et al. 2007; Roberts et al. 2011; Reinholdsson et al. 2013) and subordinately monoclinic pyrrhotite (see Dekkers 1988; 1989). Magnetic iron sulphides appeared to exist in all investigated environments, but their content strongly varied. The presence of greigite in high-susceptibility specimens may be interpreted as either an authigenic chemical precipitation (possibly supported by microbial activity) or mineralization by magnetotactic bacteria. High-susceptibility specimens were not found in this study to stand out significantly in terms of the anisotropy of susceptibility, except for samples collected within a strongly tectonically affected zone. Regarding the above, the ferromagnetic component of susceptibility was achieved presumably at the early-diagenetic stage with no preferred alignment of easy magnetization axes.

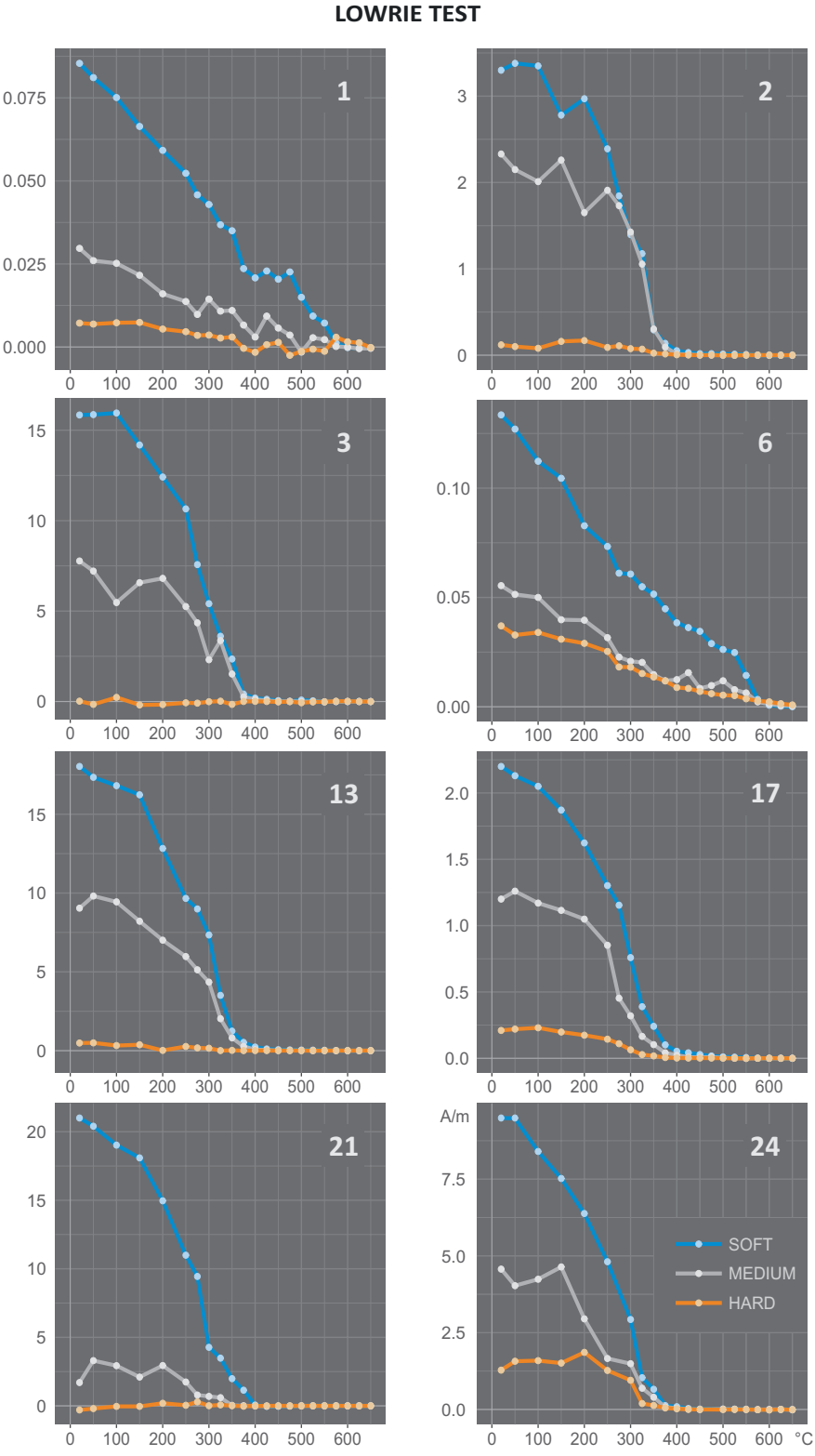

Fig. 5. Thermal demagnetization of a three-component IRM [A/m] produced by magnetizing the sample in 3.0 T along its z-axis (orange), followed by 0.4 T along the y-axis (grey), and finally 0.12 T along the x-axis (blue). For specimen details see Fig. 4A.

AMS facies

According to the mineral content discussed above, most specimens have a susceptibility controlled by paramagnetics, predominantly clay minerals. This allows for interpretation of the AMS in terms of clay particles alignment being a result of sedimentation, compaction, and tectonic reorientation. The standard cylinder-shaped specimen having above 10 cm^3 used in this study reflects the total anisotropy of many clay-, silt- and sand-sized grains, as well as other components up to a few millimetres wide, such as flora debris, muddy clasts, lithoclasts, and small concretions. It also summarizes the variability of laminations and small

bioturbations. Sedimentary structures, and other sediment variables having a size of several centimetres, may be characterized by a set of AMS specimens, referred to as *a sample* in this article and consisting of up to 25 specimens (Fig. 1). Using this approach Łoziński et al. (2016) have given the basis for the definition of AMS facies with respect to lithofacies type in the well-studied Oravica River section (Łoziński et al. 2015). The concept of AMS facies (also AMS fabrics) follows the idea of the descriptive categorization of observations and measurements, usually with some genetic interpretation, and has already been used by other authors (e.g., Garcés et al. 1996; Ort et al. 2015). In this study, AMS facies is defined by the distribution of anisotropy degree (P) and shape (T) parameters (Fig. 6). For the anisotropy determined by a given clay mineral composition, the anisotropy degree (P) parameter is dependent on the clay content and consistency of particle arrangement. The shape parameter (T) characterizes the type of particle alignment: T>0 (oblate ellipsoid) denotes preferred plane-parallel alignment (foliation), whereas T<0 (prolate ellipsoid) axis-parallel alignment (lineation). For a statistical description of specimen P and T values within a sample, median values Pm and Tm (quantile 50 %) and range indicators Pr and Tr (quantile 90 %−quantile 10 %) have been used. The range of these four values within the studied samples are given in Table 2.

All 85 AMS samples have been grouped into AMS facies (bracketed facies codes) with the focus on distinguishing previously defined lithofacies and levels of structural deformations (Fig. 7). The *consolidated* and *moderately deformed* categories were combined since they appeared to be undistinguishable in AMS fabrics. The most common AMS facies <Fm> which represents typical massive siltstones (lithofacies Fm, subordinately Fmm, and Fmc) is characterized by low anisotropies (Pm from 1.009 to 1.029) and a high shape range (Tr from 0.40 to 1.43), usually manifested by the presence of negative T values (prolate fabric) of individual specimens. This poorly fits the generally accepted sedimentary AMS fabric which is clearly anisotropic and oblate (e.g., Crimes & Oldershaw 1967, Tarling & Hrouda 1993). This may be attributed to the wide range of post-sedimentation processes including sediment drying, wetting, and bioturbation, which cause movement and reorientation of the sediment particles and decrease the general anisotropy. The group of samples with the smallest anisotropies (Pm≤1.008) has been assigned to a separate AMS facies <Fm-unc> representing deposits un- or weakly- consolidated, often porous and subjected to present-day surface processes (lithofacies Fmm and Fm). The border between facies <Fm> and <Fm-unc> is arbitrary and a range of intermediate fabrics are present. The lithofacies Fm in the tectonically deformed zone of the Červený stream appears to have reduced anisotropy shape value so that negative T values predominate (Tm from −0.38 to −0.04, <Fm-def>). The effect of a presumed horizontal compression could have overcome the original oblate anisotropy resulting in prolate fabric. Although the deformational factor is unquestionable, the AMS fabric of samples is not clearly triaxial suggesting that a ductile deformation could have occurred. The more distinct tectonic fabric is present within the tectonic zone of the Wojcieszacki stream where k1 axes are well-grouped and k2 and k3 are scattered. The lithofacies <Fm-rot> denoting the rotated fabric (k3 rotated from normal to a bedding plane position) has T values predominantly negative (Tm=−0.16) and slightly higher anisotropies than facies <Fm-def>.

The AMS facies <S> represents a sand-dominated lithofacies (mainly Sh, Sp, and St) having low oblate anisotropies (Pm from 1.017 to 1.022). Compared to facies <Fm> it has a rather narrow range of anisotropy shape values (Tr from 0.20 to 0.42) which may be attributed to the current-driven grain sorting and sedimentation giving the well-clustered AMS parameters. Additionally, the post-sedimentation processes, altering the magnetic sedimentary fabric within floodplain deposits (lithofacies Fm), could have been absent from river-channel deposits. However, a range of intermediate settings (e.g., crevasse splays and ephemeral channel deposits) is possible, so the AMS facies may be ambiguous as well. The other lithofacies deposited from the current form a continuum of AMS facies (<Hst>, <Hsl>, and <Fl>) having a clearly oblate fabric and well-clustered AMS parameters. The heterolithic lithofacies Hs may occur within various sedimentary settings, thus it has revealed two different AMS fabrics. The AMS facies <Hst> (terrestrial) has a wide range of anisotropy degree (Pr from 0.023 to 0.040) which reflects the changes of the deposition mechanism. It could have occurred within the settings of ephemeral currents, such as flood plains and ephemeral channels. In contrast, the AMS facies <Hsl> (lacustrine) is characterized by a well-grouped anisotropy degree of values (Pr from 0.011 to 0.014). In this case, the grain size and depositional mechanism (interpreted as a low-density turbidity current) do not change as much as for <Hst>. While the sand-dominated heterolithic facies <Hsl> has Pm values from 1.024 to 1.032, the silt- and clay-dominated deposits of lithofacies Hf, Fl, and CL represented by one AMS facies <Fl> (lacustrine) have higher anisotropies with Pm ranging from 1.034 to 1.041. The well-clustered AMS parameters, and clearly oblate anisotropy of <Hsl> and <Fl>, point to a stable undisturbed deposition favoured in long-lasting lakes, and thus provide a good environmental indicator. The contrasting AMS facies <CLt> (terrestrial) displays a wide range of anisotropies (Pr from 0.036 to 0.071), similar to that of facies <Hst>. The high dispersion of anisotropies may be attributed to the strong dependence of a short-lasting pond deposition to environmental fluctuations manifested by the influx of silty material (low anisotropy) and plant debris (high anisotropy). In addition, oxygen-deficient conditions in swampy areas could have favoured precipitation of magnetic minerals (mainly iron sulphides) which contribute to higher magnetic susceptibility of facies <CLt> and its anisotropy parameters. The AMS facies <CCL> represents an organic matter-abundant clayey lithofacies CCL, with the highest degree of observed anisotropy (Pm up to 1.078). The tectonically deformed AMS facies <CLt-def>, <Hsl-def>, <Fm-def> and

<Fm-rot> exhibit lower shape Tm values than their moderately deformed equivalents <CLt>, <Hsl> and <Fm>. The prolate shapes are common especially within <Fm-def> and <Fm-rot>, so the tectonic overprint appears to be strongly lithofacies-dependent.

Facies associations

The lithofacies associations and their succession supported by AMS facies analysis lead to the definition of general facies associations and allow for the interpretation of the

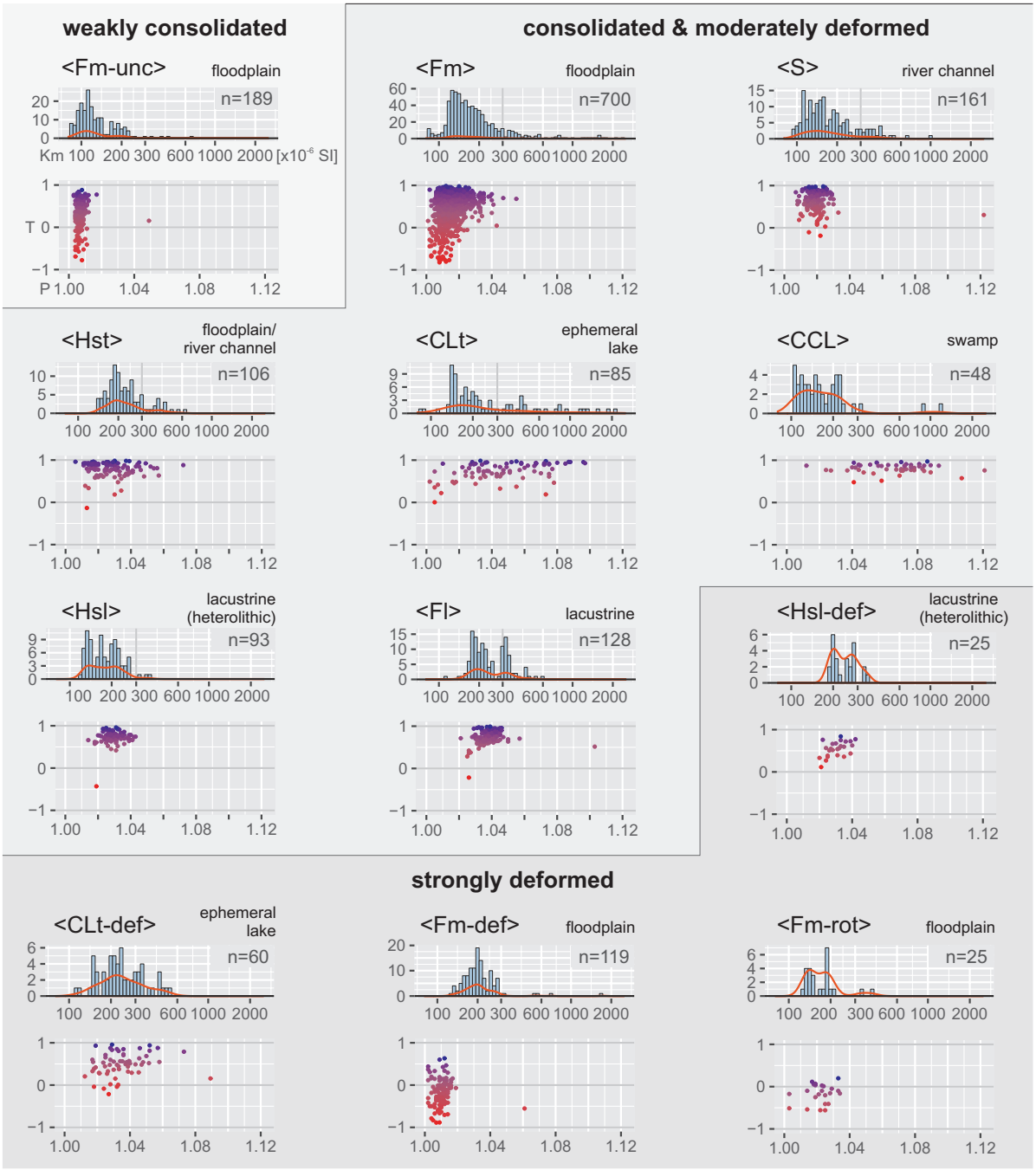

Fig. 6. The characteristics of AMS facies defined with respect to lithofacies type, inferred depositional environment and degree of deformation: mean susceptibility histograms (Km) and plots of anisotropy shape (T) towards anisotropy degree (P). The name of each group designates the lithofacies determining the AMS fabrics: CLt — claystone (terrestrial), CCL — coaly claystone, Fm - massive siltstone, Hst and Hsl — heterolithic deposits (terrestrial and lacustrine), S — massive and horizontally/trough cross-bedded sandstones, Fl — laminated siltstones and claystones. The degree of deformation other than *consolidated & moderately deformed* is denoted with: unc (weakly consolidated, undeformed, very low anisotropies P), def (tectonically induced particle reorientation; reduced shape parameter T), and rot (strong particle reorientation; partial rotation of k3 from bedding plane). Number of specimens are denoted with *n*.

Table 2: Statistical characteristics of the AMS facies: median and range values of anisotropy degree P and anisotropy shape T (see text for explanations). Unique features of individual facies are marked in bold.

AMS facies code	Lithofacies equivalent	Deformation	Pm (median)	Pr (range)	Tm (median)	Tr (range)
<Fm-unc> <Fm> <Fm-def> <Fm-rot>	Fm, Fmm, Fmc	weak moderate strong k2-k3 rotation	**1.006÷1.008** **1.009÷1.029** **1.006÷1.012** **1.022** (low)	0.003÷0.012 0.004÷0.029 0.004÷0.010 0.017	0.28 ÷ 0.68 0.03 ÷0.81 **-0.38 ÷ -0.04** **-0.16** (low)	**0.38÷1.06** **0.40÷1.43** **0.45÷0.84** **0.62** (high)
<S>	Sh, Sp, St, Hs, Fm (sandy)	weak, moderate	**1.017 ÷ 1.022** (low)	0.007÷0.019	0.51 ÷ 0.86 (high)	0.20÷0.42
<Hst>	Hs	weak, moderate	1.023÷1.030	**0.023÷0.040** (high)	0.64 ÷ 0.89	0.19÷0.29
<Hsl> <Hsl-def>	Hs	weak, moderate strong	1.024÷1.032 1.031	**0.011÷0.014** **0.016** (low)	0.70 ÷ 0.77 0.56	0.15÷0.31 0.41
<Fl>	Hf, Fl, CL	weak, moderate	1.034÷1.041	0.012÷0.017	0.61 ÷ 0.94	0.10÷0.29
<CLt> <CLt-def>	CL, Fm (clayey)	weak, moderate strong	1.034÷1.067 1.032÷1.039 (average)	**0.036÷0.071** **0.031÷0.033** **(high)**	0.70 ÷ 0.91 0.48 ÷ 0.71	0.24÷0.61 0.33÷0.78
<CCL>	CCL	weak, moderate	**1.051÷1.078** (high)	0.029÷0.032	0.79 ÷ 0.83	0.17÷0.24
<chaotic>	–	–	chaotic ellipsoid directions			

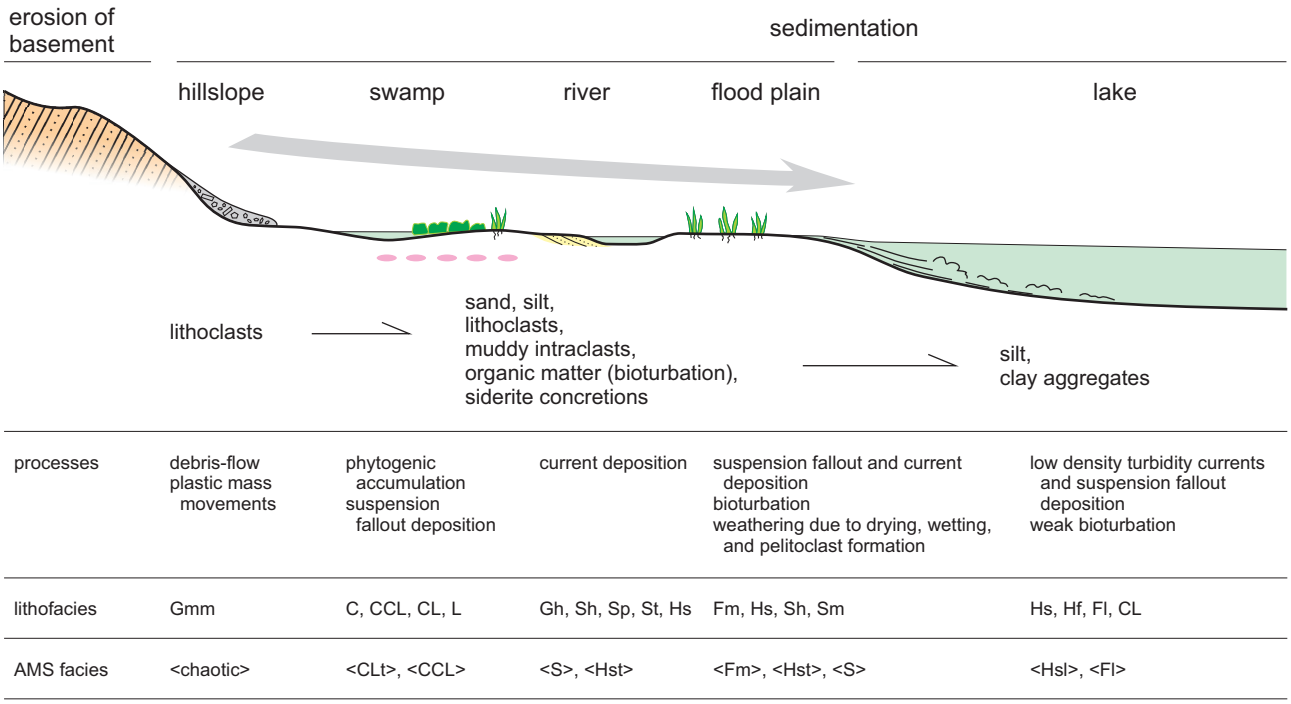

Fig. 7. Model of lateral diversification of sedimentary processes, lithofacies and AMS facies. Siliciclastic material derived from the eroded basement reaches the terrestrial settings of the basin having the form of sand and silt grains, and lithoclasts, or is reworked as muddy intraclasts. Muds on flood plains are subjected to synsedimentary weathering and bioturbation. Only fine, well-sorted grains and clay particles are brought into the lake setting and settle from low-density currents and suspension fallout. The AMS facies support the environmental interpretation, and especially help to distinguish between terrestrial and lacustrine settings (e.g., ambiguous lithofacies CL and Hs).

sedimentary environment (Table 3, Fig. 8). Tuffites being a separate facies (FA-I) have been noticed mostly near the southern margin of the basin (Bystry stream — e.g., Sikora & Wieser 1974; Czarny Dunajec river; Oravica river — Łoziński et al. 2015) and locally in the northern margin (Lipnica Mała village — Kołcon and Wagner 1991; and the Bobrov village vicinity — Beleš 1974). The lacustrine facies association (FA-II) is designated by mostly fine-grained laminated lithofacies Hf and Fl. The AMS facies <Hsl> and <Fl> provide a proper proxy in the case of indistinct sedimentary structures. These deposits crop out in the southern part of the basin only (Fig. 8) and represent stable lacustrine sedimentary conditions

over a long period. The swamp facies association (FA-III) typically inferred from abundant organic matter (CCL, C) associated with fine-grained deposits (CL, Fm) have a larger extent than the latter. The areas of low clastic input, often with stagnant water, favoured phytogenic accumulation and organic matter preservation in oxygen-deficient conditions (Bojanowski et al. 2016). The organic detritus content is marked well by a high grade of magnetic anisotropy. Within this facies association freshwater limestones may be found (Łoziński et al. 2015), but they were encountered only in the southernmost outcrops (Nové Ústie village, Oravica and Jelešňa rivers). The associations mentioned above are spatially exclusive with the weakly consolidated floodplain facies association (FA-IV). This one represents floodplain lithofacies Fm and Fmm cropping out in rather flat areas of the basin. The AMS usually reveals clearly horizontal sedimentary fabric. Deposits often exhibit considerable porosity and are affected by present-day bioturbation. Considering the above, this facies association is presumed to be the youngest of the basin sedimentary sequence and therefore determines the extent of the greatest modern subsidence. The consolidated equivalent for FA-IV is the floodplain facies association (FA-V), which is the most common in the Orava Basin. The massive lithofacies Fm and its low magnetic anisotropy suggest that the original structure has been lost due to synsedimentary weathering including the wetting-drying process and bioturbation (Wetzel & Einsele 1991). The finest organic detritus have been almost totally wiped out which points to well oxidizing conditions within exposed mudflats. In contrast, the fluvial channel facies association (FA-VI) comprises distinctly bedded sandstones and conglomerates. The AMS fabric is oblate with well-clustered anisotropy parameters. Fluvial channel deposits are not very common, but they appear throughout the whole basin. The alluvial fan facies association (FA-VII) comprises large

Table 3: Facies associations and their interpretation.

Facies associations	Dominant lithofacies	Minor lithofacies	Dominant AMS facies	Interpretation
FA-I	T		–	tuffites
FA-II	Hs, Hf, Fl, CL		<Hsl>, <Fl>	long-lasting lake
FA-III	C, CCL, CL	Fm, L	<CCL>, <CLt>	swamp
FA-IV	Fm, Fmm	Sm	<Fm>, <Fm-unc>, <S>	floodplain, weak consolidation or weathered
FA-V	Fm	Fmc, Hs, Sh, Sm	<Fm>, <Hst>, <S>	floodplain
FA-VI	Sh, Sp, St	Gh, Hs	<S>, <Hst>	sand-dominated fluvial channel
FA-VII	Gcm	Sh, Sp, St, Sm	–	gravel-dominated alluvial fan
FA-VIII	Gmm		<chaotic>	hillslope deposits (colluvium)

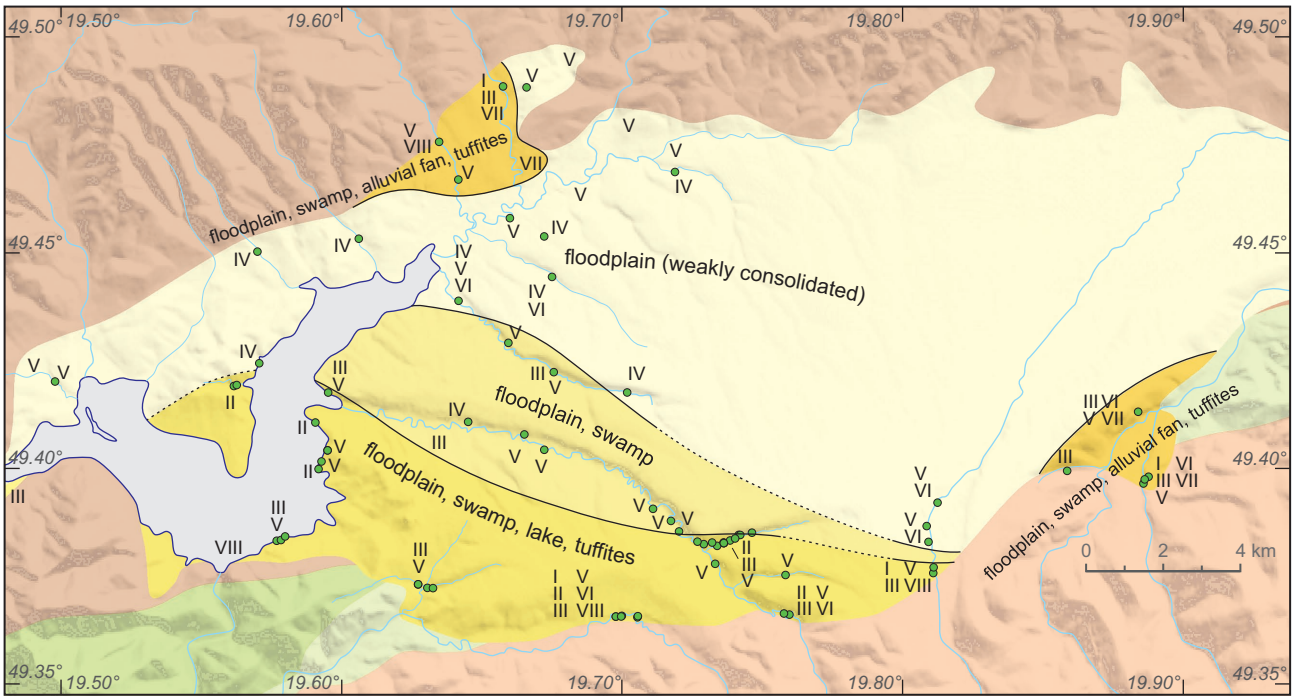

Fig. 8. Facies map of the exposed Neogene infill of the Orava Basin. Floodplain and fluvial channel deposits are widespread throughout the whole area of the basin while others are spatially restricted. The individually exposed parts of the basin are probably of a different age. The areas with abundant swamp and lake deposits as well as tuffites are interpreted as the oldest part of the basin infilling. At that time the basin could have spread further to the south (Skorušina foothills area). For facies association codes see Table 3.

bodies of conglomerates. They are exposed only on the eastern and northern margins of the basin, pointing to the location of paleosources of clastic supply and probably the synsedimentary tectonic activity. The lithofacies Gmm (FA-VIII) is interpreted as the slope debris-flow deposits with random AMS ellipsoid directions (Łoziński et al. 2016). It appears only on contact between the lowermost basin deposits and the older basement (Czarny Dunajec River, Oravica River, Orava Lake dam vicinity and Lipnica Wielka village), and probably corresponds to the onset of sedimentation when the paleorelief of the basin area had not been flattened yet.

Structural interpretation of AMS

The AMS fabric and ellipsoid axes direction constitute an excellent tool for structural analysis, especially at the early deformation stage (see discussion in Parés 2015). To ensure that the acquired AMS directions have not been induced by sampling forces (e.g., Copons et al. 1997; Shimono et al. 2014), different directions of hammering have been adopted within one sample, usually covering the range of azimuths 60÷120° wide. The k1 axes directions normal to various directions of sampling have revealed the artificially-induced ellipsoids (Fig. 9A and B) within samples Bo1, Chk1, JeQ3, Ku1, and UhQ2. This points to their weak consolidation and the lack of tectonic compression which should be much more effective than the hammering force transferred by the sampler walls' friction. Four of these samples with horizontal and subhorizontal k1–k2 plane orientations (tilted up to 12°, Fig. 10) presumably represent the youngest studied deposits located in the northern part of the basin. The k1 and k2 axes are mixed (Fig. 9D) or may be grouped indistinctly (Fig. 9C and E), which corresponds to generally sedimentary fabric. Some specimens do not pass the anisotropy tests (neither F12 nor F23, at the 99 % probability level; Jelínek 1977). In the extreme, 12 isotropic specimens (out of 25) within the sample Krz1 (lithofacies Fm) have been excluded from direction analysis and the remaining specimens represent indistinct horizontal bedding (Fig. 9C). The area of Lipnica Wielka and Lipnica Mała villages near the northern basin margin stands out for having a clearly triaxial AMS fabric and bedding tilted above 15°. However, the most numerous tectonic features are present in the southern part of the basin (Fig. 10). The AMS ellipsoid axes are predominantly triaxial or indistinctly triaxial (Fig. 9F and G), whereas sedimentary fabric is virtually absent. The bedding is commonly tilted above 10° and can be vertical within the zones affected tectonically. The Bobrov–Jelešńa zone has been identified from the vertical k1–k2 plane of AMS ellipsoids within sample Bv1 (Figs. 1 and 9H). Further investigation has confirmed a strongly inclined bedding plane (e.g., sample Bv3) with a strike of 102°. This direction trend is accurately continued on the other side of the Orava Lake by the valley of the Jelešńa River suggesting that the river may follow a tectonic lineament. The zone is accompanied by slightly inclined deposits (sample JO3 and JO6) with explicit triaxial AMS fabric with k1 oriented 120° and suggesting (together with samples Bv1 and Bv3) the NNE-trending strongest compression. The strong deformation manifested by joints, faults and a fold has been observed on the southern shore of the Orava Lake, near the Nové Ústie village. The AMS measurements have confirmed a variety of bedding orientation from gently inclined (sample Us1 and Us3) to nearly vertical (sample Us2), and k1 trending from 105° down to 70° (respectively). A similar trend of k1 axis has been found for the sample JO1 (k1 at 98°), from the eastern part of the Orava Lake shore (Fig. 10). This area has been affected by mass movements, which could have resulted in east-trending steeply inclined bedding, measured conventionally and from the AMS k1–k2 plane for sample JO2 (Fig. 9F). Samples JO4 and JO5 collected at the top of the landslide scarp are unaffected and thus provide reliable k1 directions following the discussed trend (128° and 106° respectively).

The claystones and siltstones (lithofacies CL and Fm) interbedded with fractured coals cropping out in Kovalinec and the Uhliská streams are gently tilted and locally faulted. The sample Ko2 has been interpreted as deformed claystone (AMS facies <CLt-def>) due to the decreased shape parameter T compared to undeformed claystones (Fig. 6) and a significant dispersion of the AMS ellipsoid directions (Fig. 9I) unusual for this lithofacies. Similarly, the sample Uh1 provides very poor axes grouping making the k1 direction unreliable. They have probably undergone a ductile deformation, which is additionally suggested by fluctuations of lamination observed on weathered surfaces. The neighbouring sample UhQ2 has been affected by sampling and is probably a younger, weakly consolidated deposit.

The Oravica and Jelešńa sections located at the southern border of the basin both represent moderately deformed (faulted and fractured) deposits, usually with triaxial AMS fabrics. The directions of k1 are trending at 85° in Oravica (Łoziński et al. 2016) and 108° in Jelešńa (Fig. 9G) and seem to follow the local direction of the exposed contact of the Neogene with the older basement. The strongly deformed zone of Červený stream located north of the Oravica and Jelešńa sections has been identified from numerous faults and vertical or steep bedding planes striking at azimuth of 60° and confirmed by the AMS k1–k2 planes (samples Ce9 and Ce10, Fig. 11A). Most outcrops represent massive lithofacies Fm, so the AMS measurements of 11 samples have been done to trace the extent and the character of this zone. It has turned out that samples (JeQ2, Ce3, and Ce4) collected north of the vertically bedded outcrop (and north of 60°-trending line following the stream valley) are gently dipping in the same direction (305/21÷24) and have W–E trending k1 axes. The samples south of this outcrop are either unusually south-eastward tilted 25÷50° (Ce6 and Ce11) or represent the AMS fabric dominated by prolate shapes (Ce7, Je11; Figs. 9J, 11C). The latter may represent massive lithofacies Fm with originally very weak oblate anisotropy, therefore easily undergoing deformation to become prolate. The ductile deformation observed in claystones and siltstones (Fig. 11B) could have also affected samples Ce7 and Je11 resulting in prolate shapes. Similarly to

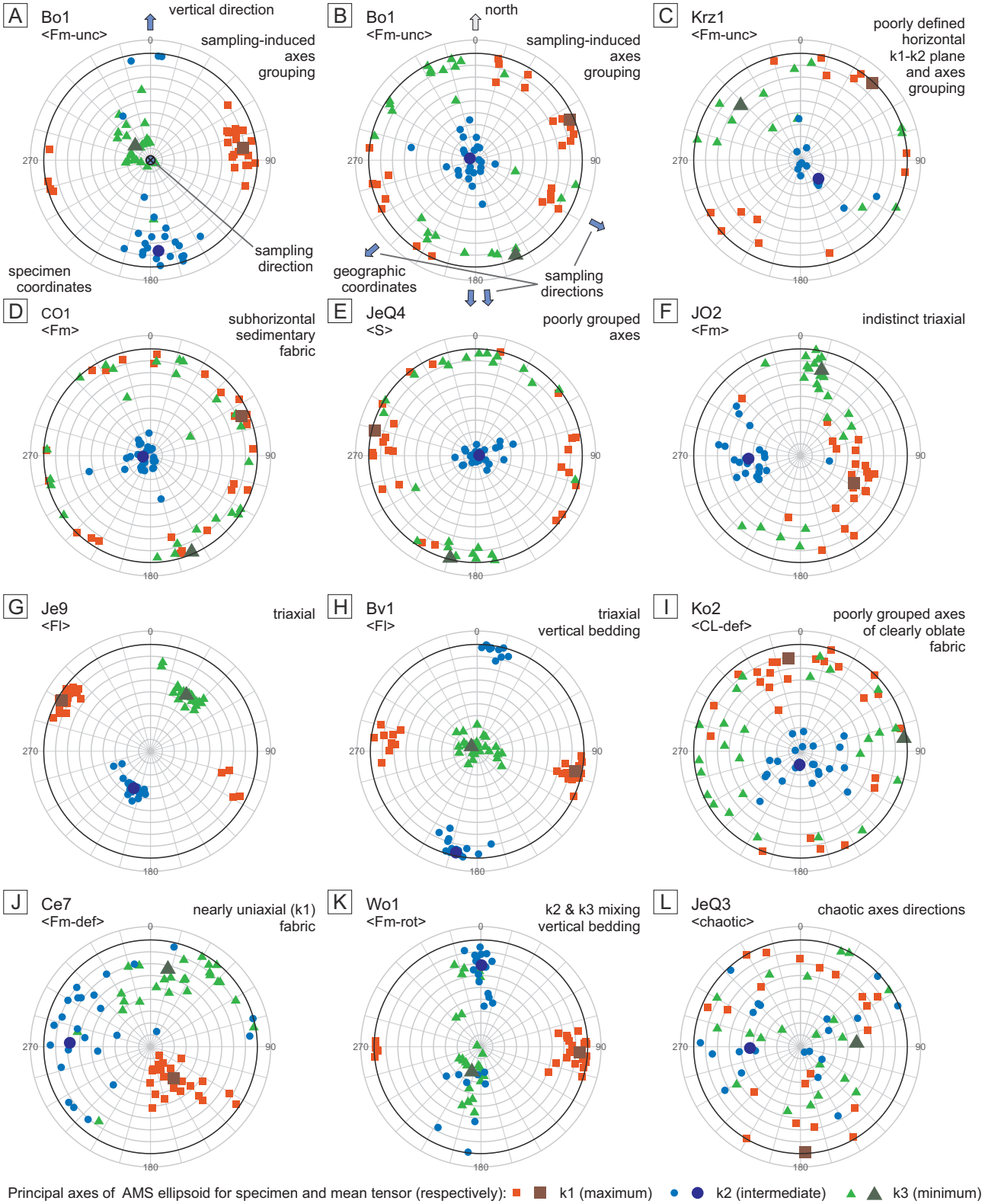

Fig. 9. The lower hemisphere's equal-area projection of the specimen AMS ellipsoid axes within individual samples. The effect of sample-induced axes grouping may be verified by applying a multi-directional sampling. The projection in a specimen coordinate system (**A**) reveals k1 clustering in a position normal to the direction of sampling (A and B). The variety of axes clustering depending on the deformation type and primary anisotropy degree are presented in a geographic coordinate system in Figs. **B**–**L** (see text for explanations). The sample name and AMS facies (in brackets) are given in the left upper corner of each plot.

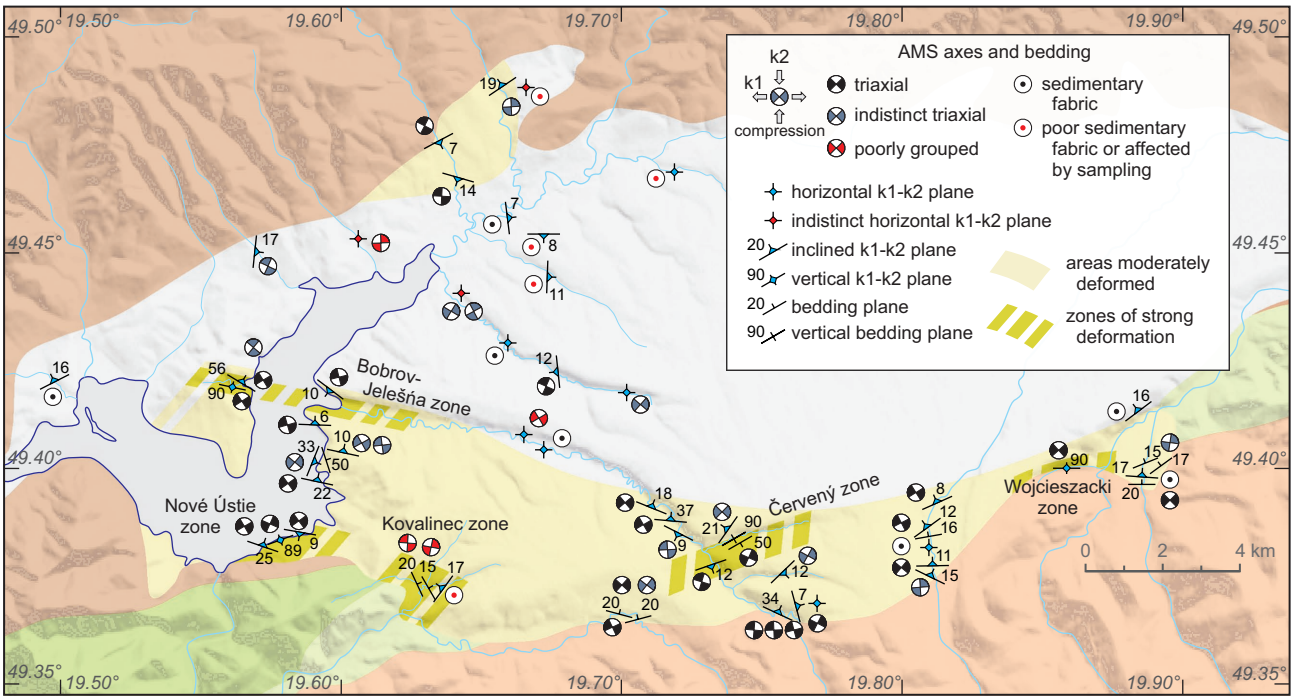

Fig. 10. The structural aspects of the mean AMS tensor axes orientation and their interpretation in terms of bedding and 2-dimensional direction of the strongest compression.

samples in the north of the tectonically affected area, the samples Ce6 and Ce11 have a W–E trending k1 axes giving the N–S the main compression axis. This combined with the general 60°-trend of the whole deformational zone indicates a probable sinistral strike-slip fault zone.

The outcrops of the Czarny Dunajec river valley exhibit moderately deformed to undeformed deposits slightly tilted (up to 16°) towards the north and north-west. The k1 directions change from the parallel to the basin margin (sample CD1), through W–E trending (samples CD2_1 and CD2_2) towards ESE-trending (samples CD4, and CD5). The north- (sample By2) and northwestward (By1 and By3) tilt and k1 axes oriented W–E have also been noted in the Bystry stream section.

The extreme deformation has been observed in the neighbouring Wojcieszacki stream. The observed vertical bedding of the coal seam has been confirmed by predominantly vertically oriented k1–k2 plane of the AMS ellipsoid (Fig. 9K) within siltstones and claystones (lithofacies Fm and subordinately CL). However, a few k3 directions are mixed with k2 directions creating a picture of transitional ellipsoid orientations towards the totally tectonic fabric, characterized by prolate shapes and axis k3 directed along the strongest compression rather than normal to bedding plane (AMS facies <Fm-rot>).

The variety of AMS fabrics ends with samples OrGmm, JeQ3, and LM2 (Fig. 9L), which have chaotic axis directions, but maintaining the anisotropy shape and degree parameters typical for their lithofacies. These have been interpreted as deposits affected by ductile mass movements keeping the original sediment structure at the scale of millimetres, but moving and rotating fragments at the scale of several centimetres.

Discussion

Lithofacies and tectonic deformations in AMS measurements

The AMS facial model presented in this paper is based on the distribution of anisotropy degree and shape parameters within a sample represented by four variables: Pm, Pr, Tm and Tr. Traditionally, the prolate shapes (Tm<0) have been indicative of grain orientation being either tectonic or current-driven (e.g., Crimes & Oldershaw 1967). This study has confirmed that deformations diminish the anisotropy shape parameter, although the AMS fabrics vary strongly with respect to lithofacies (Fig. 6). The lithofacies Fm appears to be most vulnerable to deformational overprint. Specimens from this lithofacies may acquire partially prolate shapes due to sampling forces and weak deformations (AMS facies <Fm-unc> and <Fm>), while other lithofacies remain oblate even within tectonic zones. This vulnerability may be attributed to low original anisotropy gained presumably in a range of early post-depositional processes experienced by exposed fresh muds. This shows that the precise estimation of the degree of deformation is ambiguous if the sedimentary factor is unknown. However, it seems that some lithofacies may still be identified using AMS parameters only (Fig. 6).

The directions of the AMS have been interpreted as tectonic rather than sedimentary. Maximum and intermediate axes are

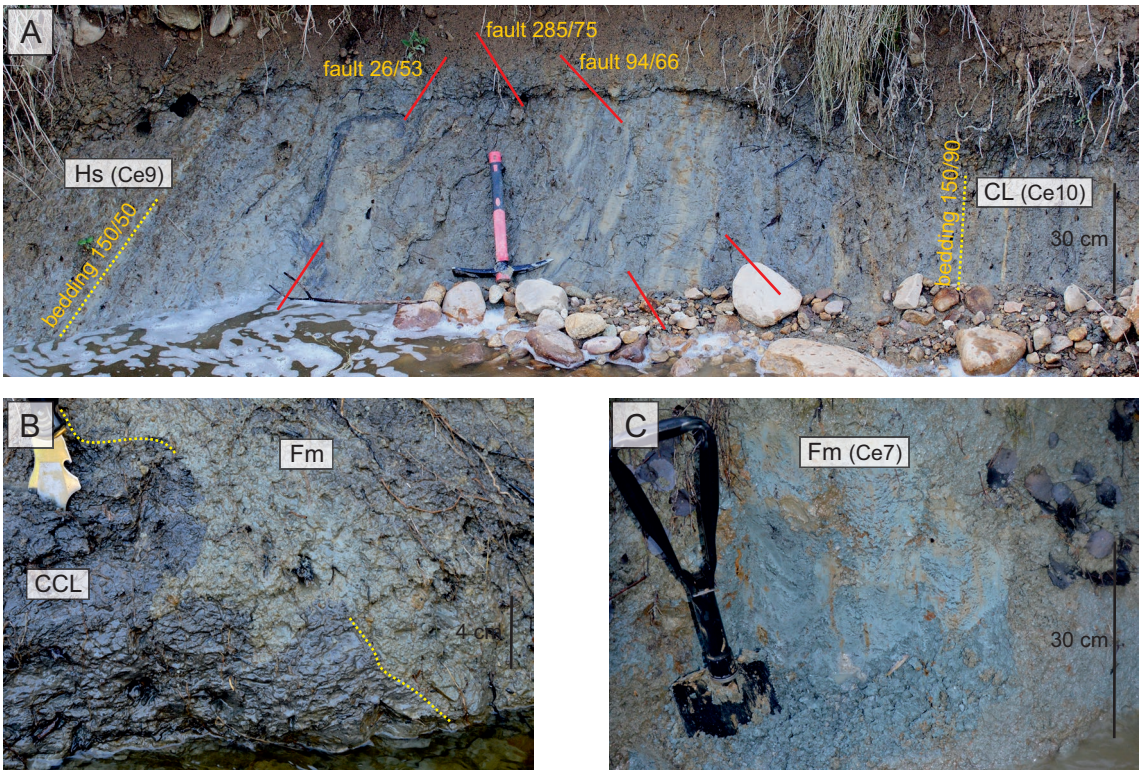

Fig. 11. Tectonic deformations within the Neogene fine clastics of the Orava Basin. AMS sample names are shown in brackets. **A** — Strongly inclined to vertical position of claystones (lithofacies CL) and sandstone-dominated heterolithic deposits (lithofacies Hs) indicates a significant deformation zone. Deposits are strongly compacted and faulted (Červený Stream). **B** — Ductile deformation resulted in irregular contact of coaly claystones (lithofacies CCL) and clayey siltstones (lithofacies Fm) (Červený Stream). **C** — Massive siltstones (lithofacies Fm) exhibit neither sedimentary, nor tectonic structures which have been inferred from the AMS measurements.

either mixed (mostly in the northern part of the basin) or represent a remarkably constant basinal trend (southern part of the basin), unusual for a fluvial-dominated environment characterized by fluctuating transport directions. This may be due to clay minerals contributing significantly to the magnetic anisotropy, which have probably been deposited as muddy clasts not favouring the current's direction. Also, the classical interpretation of sedimentary grain imbrication (e.g., Rees 1961; Crimes & Oldershaw 1967; Hamilton 1967; Rees & Woodall 1975) could not have been applied because it requires comparison of magnetic foliation with a bedding plane that was often undetermined or uncertain.

Considerable variations of the AMS parameters with respect to lithofacies indicate the significance of lithofacies-oriented sampling, a statistical approach and large datasets of measurements. The measured AMS of a specimen quantifies the alignment of sediment particles at a scale of millimetres (specimen-scale), while the homogeneity of the sediment over tens of centimetres (sample-scale) may be obtained from a multispecimen representation of each lithofacies. These two scales may be considered in terms of a time span needed to deposit a given thickness of sediment. The specimen-scale result represents a relatively short time of sedimentation and characterizes a settling mechanism, mineral composition and grain sorting. Accordingly, the sample-scale result shows the stability of sedimentary conditions over a long time with the exception for beds deposited quickly in one depositional event (e.g., AMS facies <S>). In fine-grained deposits the homogeneity has been noticed within the AMS facies <Hsl> and <Fl> being interpreted as deposits from lakes (lithofacies CL, Fl, Hf, and Hs), where the sedimentary environment enables long-term undisturbed sedimentation. It appears that all typically current-driven sediments (AMS facies <S> and <Hsl>) show good clustering of P and T parameters (low Pr and Tr). The stronger the current, the lower the anisotropy degree (Pm), probably due to the lower content of anisotropic clay minerals. This observation is contrary to deep-sea sediments affected by bottom currents where a stronger current is thought to align ferromagnetic grains more effectively (Ellwood & Ledbetter 1977; Joseph et al. 1998). In contrast, inhomogeneous AMS facies <Hst>, <CLt>, and <CCL> indicate the sedimentary conditions undergoing fluctuations or being affected by special sedimentary events (e.g., floods). These conditions are met within a river setting, especially within ephemeral channels, local ponds, and overbanks where crevasse splay is deposited (lithofacies Hs and CL). Swamp deposition may also be easily affected by water table change or by siliciclastic influx during floods (lithofacies CL and CCL). The AMS characteristics of a sample are found at this point to be a useful tool in distinguishing between lacustrine

and terrestrial settings of ambiguous lithofacies Hs and CL. The separate group is represented by the AMS facies <Fm> usually having low anisotropy (Pm) and low shape (Tm) values. This has been attributed to post-depositional weathering (drying, wetting, and bioturbation) presumably destroying the original sedimentary structure (Wetzel & Einsele 1991).

The evolution of the Orava Basin

The facial scheme for the Orava Basin shows the spatial differentiation of facies associations (Fig. 8). Different sedimentary conditions could have taken place in the north and south during the basin's development, but it can also be the case of stronger erosion in the south uncovering the older part of the sedimentary sequence. The conglomerate alluvial fan facies (Gcm) is a good premise for the proximity of a highland hilly area and thus it indicates the zones of basin paleomargins. These facies have been noted at the northernmost part of the basin near Lipnica Mała village and near the eastern margin, especially building up of the large Domański Wierch cone (Tokarski et al. 2012, 2016). The gravelly facies (except for Gmm) are missing in the western part and primarily all along the present-day southern basin margin (Fig. 8). On the other hand, the lacustrine facies are found only in the southern basin area and the transport direction measured in the Oravica River section (Łoziński et al. 2015) being towards S and SW points to a subsidence centre in the area of the present-day Skorušina foothills. The uplift of Paleogene rocks in this area makes the Orava Basin inversion in the south very probable, as has already been suggested by other researchers (Nagy et al. 1996; Tokarski et al. 2012; Łoziński et al. 2015). This is further supported by the contemporary hilly terrain morphology in the area south of the line of the Bobrov–Chyżne–Chochołów villages. The age of the southernmost deposits is weakly constrained, but it has been estimated to be Sarmatian in the vicinity of Nové Ústie (Nagy et al. 1996). The palynological investigation of Neogene deposits (Oszast & Stuchlik 1977) has shown a progressive climate shift from warm and humid to temperate and dry, which can be associated with the termination of the Middle Miocene Climatic Optimum (Zachos et al. 2001) towards the cool climate in the Quaternary. Favourable conditions for peat development could have existed in the Middle Miocene, and may be linked with the abundant coal seams in the southern part of the basin and in the lower part of the basin filling (borehole Czarny Dunajec-IG1; Watycha 1971). This area of the basin is also characterized by locally occurring siderite concretions related to swamps (Bojanowski et al. 2016), freshwater limestones, and tuffite intercalations probably related to the Sarmatian stage of volcanic activity in the Western Carpathians (Vass et al. 1988). These lithologies are absent in the northern part of the basin (Fig. 8) where the upper part of the basin sequence crops out. The inversion process also has regional implications. The Skorušina and Gubałówka foothills were proposed by Watycha (1976a) as a barrier which blocked material supply from the Tatra Mts in the Neogene. However, the inferred lack of such a barrier in the Sarmatian along with the absence of this material in the basin suggests that the Tatra Mts might not have been exposed enough yet although they were already uplifted (Śmigielski et al. 2016).

The deformation inferred from the AMS measurements provides a picture of a predominantly N to NE trending strongest compression axis in the south part of the basin (Fig. 10). The local deviations may be attributed to faulting and the impact of basin marginal zones. The recorded stress may depict the tectonic regime of either the basin opening or its inversion, but the tectonic AMS fabric appearing predominantly within the uplifted southern area makes the second hypothesis more probable. Moreover, Mattei et al. (1997) suggested that the magnetic lineation (k1 direction) parallel to dip direction of bedding (perpendicular to normal faults) is characteristic for tilted bedding in an extensional regime, while lineation perpendicular to dip direction denotes a shortening in the folded strata. In the southern part of the Orava Basin the magnetic lineation has a prevailing WNW–ESE trend, which, compared with a similar trend of southern basin-bounding faults (Pomianowski 2003, Fig. 12) and bedding tilted northward, suggests that the inversion could have taken place in a N to NE-trending compressional regime, resulting in a gradual uplifting of the southernmost part of the basin. In this sense, the present-day basin geometry may be treated as an asymmetrical or half- graben (Pospíšil 1993 in Gross et al. 1993b), which seems to be a common trend in other intramontane basins, such as the Nowy Targ Basin and Turiec Basin (Pomianowski 2003; Kováč et al. 2011). The acquired direction of compression is in accordance with the NE- and NNE-trend inferred from fractured clasts (Tokarski & Zuchiewicz 1998), although this direction could have been rotated (Baumgart-Kotarba et al. 2004; Tokarski et al. 2016). The uplift has been accommodated at the basin margins by dip-slip and strike-slip movements (Fig. 12) probably along regional reactivated strike-slip fault zones (e.g., Myjava Fault, also referred to as Orava Fault; Bac-Moszaszwili 1993; Baumgart-Kotarba et al. 2004). The intrabasinal fault zones, Bobrov–Jelešńa and Červený (introduced previously as topolineaments, e.g. Łój et al. 2007), could have had a significant dip-slip component together with a strike-slip movement of a second-order with respect to regional faults. The inferred extent of the basin inversion is limited in the north approximately by the Chochołów–Chyżne–Bobrov–Vavrečka line.

The Orava Basin represents an important element of the Carpathian structural domain recording the neo-Alpine stage of deformation. Its southern part has shown a considerable tectonic contribution to the magnetic fabric, partly due to weak compaction and cementation of sediments. In turn, the rocks of the Skorušina foothills adjacent to the Orava Basin have revealed sedimentary or weakly deformed AMS fabric resulting from NW–SE shortening (Hrouda & Potfaj 1993). Such a trend corresponds well with NE-trending magnetic lineations within the neighbouring area of the Magura Unit

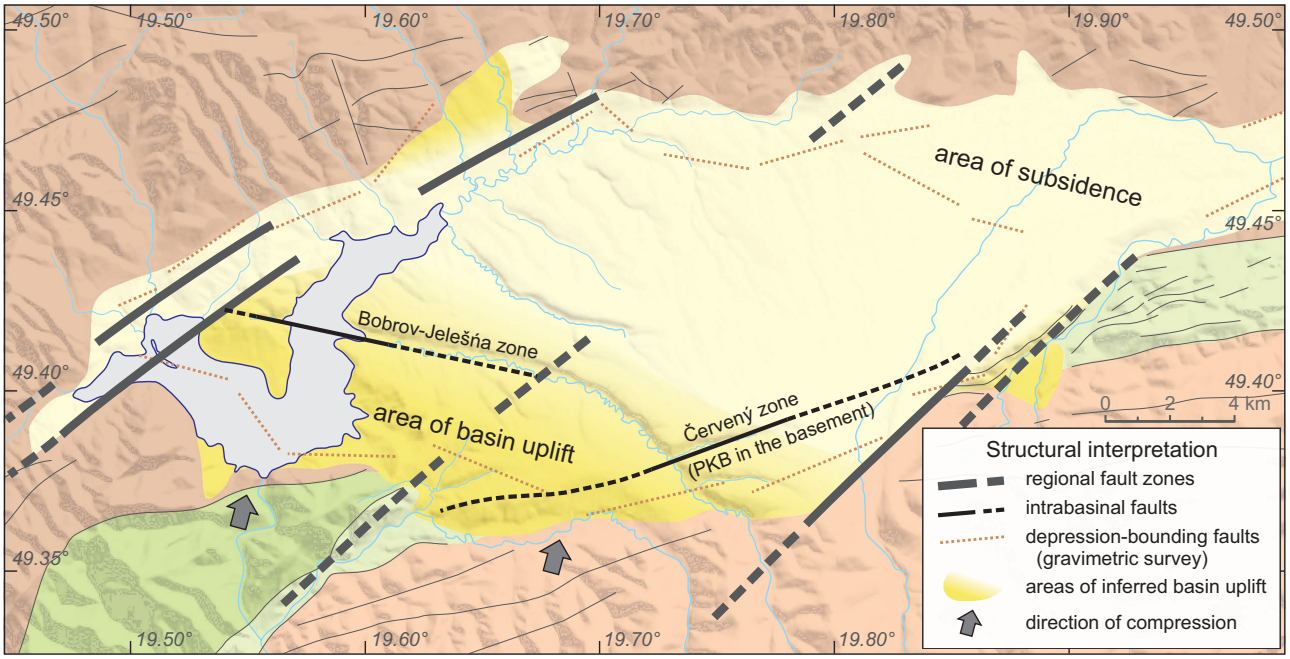

Fig. 12. Interpretation of the Orava Basin structural framework during its inversion. The basin is divided by strike-slip NE-trending fault zones into independent blocks cut by secondary-order intrabasinal faults and deformation zones (observed). The southern central part of the basin could have undergone an uplift in the NNE-trending compression regime. The arrangement of western and eastern marginal parts is determined by strike-slip zones and the movement of surrounding structural blocks. Depression-bounding faults after Pomianowski (2003).

representing relatively weakly deformed rocks and interpreted as a tectonically passive element during folding and thrusting (Hrouda et al. 2009; Márton et al. 2009). These results from older units and the obtained N to NE trending compression in the Orava Basin point to a major shift of the directions of regional stress field during the Neogene. According to many authors (e.g., Aleksandrowski 1985; Pešková et al. 2009) this change could have taken place in the Early/Middle Miocene. However, it was also suggested that the basin uplift, which could have occurred after the tectonic regime change, has continued since the Late Pliocene/Early Quaternary until the present-day (Baumgart-Kotarba 1996; Nagy et al. 1996; Tokarski et al. 2012). The direction of strongest compression suggested in this paper is supported by the similar NNE-trending contemporary thin-skin compressional regime resulting from movement of the ALCAPA unit (Jarosiński 1998; Zuchiewicz et al. 2002).

Conclusions

- A detailed scheme of 17 lithofacies representing predominantly fine-clastic deposits has been defined for the whole area of the Orava Basin.
- Median and range values of anisotropy degree (P) and shape (T) within individual sampled locations have been used to distinguish 12 AMS facies with respect to the sedimentary environment and deformation intensity. The magnetic method proved to be very effective in analysing weakly deformed fine-clastic terrestrial deposits often lacking macroscopic sedimentary features.
- Mapping of the basin area using lithofacies and AMS facies allowed us to mark the extent of the basin inversion. The result supports the hypothesis of a significantly larger basin extent in the south followed by an uplift and a complete removal of deposits in the area of the present-day Skorušina foothills.
- AMS measurements enabled us to identify two intrabasinal fault zones: Bobrov–Jelešńa and Červený. The latter points to the reactivation of faults related to the Pieniny Klippen Belt in the basement after basin sedimentation.
- The structural framework for the inversion is comprised of the regional NE-trending strike-slip fault zones together with the secondary transverse faults (e.g., Bobrov–Jelešńa and Červený) dividing the basin infilling into independently uplifted blocks.
- AMS ellipsoid directions obtained from the uplifted southern part of the basin show that the inversion has undergone compression in the NNE-trending thin-skin presumably related to the northward advance of the ALCAPA plate.

Acknowledgements: The study was financed by the National Science Centre (NCN) grant no. 2011/01/B/ST10/07591. The authors are pleased to offer special thanks to Prof. František Hrouda, Dr. Alexander Nagy and Dr. Petr Pruner (reviewers), Prof. Andreas Wetzel, Dr. Michal Šujan, Radosław Wasiluk and Katarzyna Dudzisz who have greatly contributed to this research with their advice, discussions, and archived data collection.

References

Aleksandrowski P. 1985: Structure of the Mt. Babia Góra region, Magura Nappe, Western Outer Carpathians: An interference of West and East Carpathian fold trends. *Ann. Soc. Geol. Pol.* 55, 375–422 (in Polish with English summary).

Baas J. H., Hailwood E. A., McCaffrey W. D., Kay M. & Jones R. 2007: Directional petrological characterisation of deep-marine sandstones using grain fabric and permeability anisotropy: methodologies, theory, application and suggestions for integration. *Earth-Sci. Rev.* 82, 1, 101–142.

Babinszki E., Márton E., Márton P. & Kiss L. F. 2007: Widespread occurrence of greigite in the sediments of Lake Pannon: Implications for environment and magnetostratigraphy. *Palaeogeogr. Palaeoclimatol. Palaeoecol.* 252, 3, 626–636.

Bac-Moszaszwili M. 1993: Structure of the western termination of the Tatra massif. *Ann. Soc. Geol. Pol.* 63, 1–3, 167–193 (in Polish with English summary).

Baumgart-Kotarba M. 1996: On origin and age of the Orava Basin, West Carpathians. *Stud. Geomorph. Carpatho-Balcanica* 30, 101–116.

Baumgart-Kotarba M. 2001: Continuous tectonic evolution of the Orava basin from Late Badenian to the present-day? *Geol. Carpath.* 52, 103–110.

Baumgart-Kotarba M., Michalik M., Paszkowski M., Świerczewska A., Szulc J. & Uchmann A. 1996: Provenance and age of coarse clastic alluvial deposits at Čimhova in the Orava Basin, Western Carpathians, Slovakia. *Pol. Miner. Soc., Spec. Pap.* 7, 68–72.

Baumgart-Kotarba M., Marcak H., Márton E. & Imre G. 2004: Rotation along transverse transforming Orava strike-slip fault in the light of geomorphological, geophysical and paleomagnetic data (Western Carpathians). *Geol. Carpath.* 55, 219–226.

Beleš F. 1974: Occurrence of bentonite in the Orava river basin. *Mineralia Slovaca* 6/2, 155–157. (in Slovak with English summary).

Birkenmajer K. 1954: Geological investigations of Podhale Neogene (Central Carpathians). *Bull. Geol. Inst, Warsaw* 86, 59–79 (in Polish with English summary).

Birkenmajer K. 1960: Geology of the Pieniny Klippen Belt of Poland. *Jahrb. Geol. Bundesanst.* 103: 1–36.

Birkenmajer K. 1978. Neogene to Early Pleistocene subsidence close to the Pieniny Klippen Belt, Polish Carpathians. *Stud. Geomorph. Carpatho-Balcanica* 12, 17–28.

Birkenmajer K. & Oszczypko N. 1989: Cretaceous and Palaeogene lithostratigraphic units of the Magura Nappe, Krynica Subunit, Carpathians. *Ann. Soc. Geol. Pol.* 59, 145–181.

Biró T., Karátson D., Márton E., Józsa S. & Bradák B. 2015: Paleoflow directions of a subaqueous lahar deposit around the Miocene Keserűs Hill lava dome complex (North Hungary) as constrained by photo-statistics and anisotropy of magnetic susceptibility (AMS). *J. Volcanol. Geotherm. Res.* 302, 141–149.

Bojanowski M., Jaroszewicz E., Košir A., Łoziński M., Marynowski L., Wysocka A. & Derkowski A. 2016: Root-related rhodochrosite and concretionary siderite formation in oxygen-deficient conditions induced by a ground-water table rise. *Sedimentology* 63, 523–551.

Cieszkowski M. 1995: Marine Miocene deposits close to Nowy Targ and their importance for determining age of the Orava-Nowy Targ Basin. *Kwartalnik AGH Geologia* 21, 2, 153–168 (in Polish with English summary).

Cieszkowski M., Oszczypko N. & Zuchiewicz W. 1989: Upper Cretaceous siliciclastic carbonate turbidites at Szczawa, Magura Nappe, West Carpathians, Poland. *Bull. Pol. Acad. Sci., Earth Sci.* 37, 231–245.

Copons R., Parés J.M., Dinarès-Turell J. & Bordonau J. 1997: Sampling Induced AMS in Soft Sediments: A Case Study in Holocene Glaciolacustrine Rhythmites from Lake Barrancs (Central Pyrenees, Spain). *Phys. Chem. Earth* 22, 1–2, 137–141.

Crimes T. P. & Oldershaw M. A. 1967: Palaeocurrent determinations by magnetic fabric measurements on the Cambrian rocks of St. Tudwal's Peninsula, North Wales. *Geol. J.* 5, 2, 217–232.

Dekkers M. J. 1988: Magnetic properties of natural pyrrhotite Part I: Behaviour of initial susceptibility and saturation-magnetization-related rock-magnetic parameters in a grain-size dependent framework. *Phys. Earth Planet. Inter.* 52, 3-4, 376–393.

Dekkers M. J. 1989: Magnetic properties of natural pyrrhotite. II. High-and low-temperature behaviour of Jrs and TRM as function of grain size. *Phys. Earth Planet. Inter.* 57, 3-4, 266–283.

Ellwood B. B. & Ledbetter M. T. 1977: Antarctic bottom water fluctuations in the Vema Channel: effects of velocity changes on particle alignment and size. *Earth Planet. Sci. Lett.* 35, 2, 189–198.

Eyles N., Day T. E. & Gavican A. 1987: Depositional controls on the magnetic characteristics of lodgement tills and other glacial diamict facies. *Can. J. Earth Sci.* 24, 12, 2436–2458.

Garcés M., Parés J.M. & Cabrera L. 1996: Inclination error linked to sedimentary facies in Miocene detrital sequences from the Vallès-Penedès Basin (NE Spain). *Geol. Soc. London, Spec. Publ.* 105, 91–99.

Garecka M. 2005: Calcareous nannoplankton from the Podhale Flysch (Oligocene-Miocene, Inner Carpathians, Poland). *Stud. Geol. Pol.* 124, 353–370.

Graham J. W. 1954: Magnetic susceptibility anisotropy, an unexploited petrofabric element. *Geol. Soc. Am. Bull.* 65, 12, 1257–1258.

Gravenor C. P. & Wong T. 1987: Magnetic and pebble fabrics and origin of the Sunnybrook Till, Scarborough, Ontario, Canada. *Can. J. Earth Sci.* 24, 10, 2038–2046.

Gross P., Filo I., Halouzka R., Haško J., Havrila M., Kováč P., Maglay J., Mello J. & Nagy A. 1993a: Geological map of southern and eastern part of Orava. *State Geol. Inst. of Dionýz Štúr*, Bratislava.

Gross P., Köhler E., Haško J., Halouzka R., Mello J. & Nagy A. 1993b: Geology of southern and eastern Orava. *State Geol. Inst. of Dionýz Štúr*, Bratislava, 1–319 (in Slovak).

Hamilton N. 1967: The effect of magnetic and hydrodynamic control on the susceptibility anisotropy of redeposited silt. *J. Geol.* 75, 6, 738–743.

Hrouda F. 1982: Magnetic anisotropy of rocks and its application in geology and geophysics. *Geophysical Surveys* 5, 37–82.

Hrouda F. 2010: Modelling relationship between bulk susceptibility and AMS in rocks consisting of two magnetic fractions represented by ferromagnetic and paramagnetic minerals — Implications for understanding magnetic fabrics in deformed rocks. *J. Geol. Soc. India* 75, 1, 254–266.

Hrouda F. & Potfaj M. 1993: Deformation of sediments in the post-orogenic Intra-Carpathian Paleogene Basin as indicated by magnetic anisotropy. *Tectonophysics* 224, 4, 425–434.

Hrouda F., Jelínek V. & Zapletal K. 1997: Refined technique for susceptibility resolution into ferromagnetic and paramagnetic components based on susceptibility temperature-variation measurement. *Geophys. J. Int.* 129, 3, 715–719.

Hrouda F., Krejčí O., Potfaj M. & Stráník Z. 2009: Magnetic fabric and weak deformation in sandstones of accretionary prisms of the Flysch and Klippen Belts of the Western Carpathians: Mostly offscraping indicated. *Tectonophysics* 479, 3, 254–270.

Jankowski L. & Margielewski W. 2014: Structural control on the Outer Carpathians relief — a new approach. *Przegl. Geol.* 62, 1, 29–35 (in Polish with English summary).

Jarosiński M. 1998: Contemporary stress field distortion in the Polish part of the Western Outer Carpathians and their basement. *Tectonophysics* 297, 1, 91–119.

Jelínek V. 1977: The statistical theory of measuring anisotropy of magnetic susceptibility of rocks and its application. *Geofyzika*, Brno, 1–88.

Jelínek V. & Kropáček V. 1978: Statistical processing of anisotropy of magnetic susceptibility measured on groups of specimens. *Studia Geophys. Geod.* 22, 50–62.

Joseph L. H., Rea D. K. & van der Pluijm B. A. 1998: Use of grain size and magnetic fabric analyses to distinguish among depositional environments. *Paleoceanography* 13, 5, 491–501.

Kanamatsu T. & Herrero-Bervera E. 2006: Anisotropy of magnetic susceptibility and paleomagnetic studies in relation to the tectonic evolution of the Miocene–Pleistocene accretionary sequence in the Boso and Miura Peninsulas, central Japan. *Tectonophysics* 418, 1, 131–144.

Klappa C. F. 1980: Rhizoliths in terrestrial carbonates: classification, recognition, genesis and significance. *Sedimentology* 27, 613–629.

Kołcon I. & Wagner M. 1991: Brown coal from Neogene sediments of the Orawa-Nowy Targ basin — petrological study. *Geol. Quarterly* 35, 3, 305–322 (in Polish with English summary).

Kováč M., Nagymarosy A., Soták J. & Šutovská K. 1993: Late Tertiary paleogeographic evolution of Western Carpathians. *Tectonophysics* 226, 401–415.

Kováč M., Hók J., Minár J., Vojtko R., Bielik M., Pipík R., Rakús M., Kráľ J., Šujan M. & Králiková S. 2011: Neogene and Quaternary development of the Turiec Basin and landscape in its catchment: a tentative mass balance model. *Geol. Carpath.* 62, 4, 361–379.

Kukulak J. 1998: Sedimentary characteristics of the topmost deposits, Domański Wierch alluvial cone (Neogene/Pleistocene), Orava Depression, Polish Carpathians. *Stud. Geol. Pol.* 111, 93–111 (in Polish with English summary).

Kukulak J. 1999: Orientation of joints and faults in the SE part of the Orawa Depression. *Przegl. Geol.* 47, 11, 1021–1026 (in Polish with English summary).

Lowrie W. 1990: Identification of ferromagnetic minerals in a rock by coercivity and unblocking temperature properties. *Geophys. Res. Lett.* 17, 159–162.

Łoziński M., Wysocka A. & Ludwiniak M. 2015: Neogene terrestrial sedimentary environments of the Orava-Nowy Targ Basin: a case study of the Oravica River section near Čimhová, Slovakia. *Geol. Quarterly* 59, 1, 21–34.

Łoziński M., Ziółkowski P. & Wysocka A. 2016: Lithofacies and terrestrial sedimentary environments in AMS measurements: case study from Neogene of Oravica River section, Čimhová, Slovakia. *Geol. Quarterly* 60, 2, 259–272.

Łój M., Madej J., Porzucek S. & Zuchiewicz W. 2007: Young tectonics of the Orava Basin and southern portion of the Magura Nappe, Polish western Carpathians, in the light of gravity studies: a new research proposal. *Studia Quaternaria* 24, 53–60.

Malata E., Malata T. & Oszczypko N. 1996: Litho- and biostratigraphy of the Magura Nappe in the eastern part of the Beskid Wyspowy Range (Polish Western Carpathians). *Ann. Soc. Geol. Pol.* 66, 269–283.

Márton E., Rauch-Włodarska M., Krejčí O., Tokarski A. K. & Bubík M. 2009: An integrated palaeomagnetic and AMS study of the Tertiary flysch from the Outer Western Carpathians. *Geophys. J. Int.* 177, 3, 925–940.

Mattei M., Sagnotti L., Faccenna C., & Funiciello R. 1997: Magnetic fabric of weakly deformed clay-rich sediments in the Italian peninsula: relationship with compressional and extensional tectonics. *Tectonophysics* 271, 1, 107–122.

Mazzoli S., Szaniawski R., Mittiga F., Ascione A. & Capalbo A. 2012: Tectonic evolution of Pliocene–Pleistocene wedge-top basins of the southern Apennines: new constraints from magnetic fabric analysis. *Canadian Journal of Earth Sciences* 49, 3, 492–509.

Miall A.D. 2000: Principles of Sedimentary Basin Analysis. *Springer-Verlag*, Berlin–Heidelberg–New York, 1–616.

Miall A.D. 2006: The Geology of Fluvial Deposits: Sedimentary Facies, Basin Analysis and Petroleum Geology. *Springer*, Berlin, 1–582.

Nagy A., Vass D., Petrik F. & Pereszlényi M. 1996: Tectogenesis of the Orava Depression in the light of latest biostratigraphic investigations and organic matter alteration studies. *Slovak Geol. Mag.* 1, 49–58.

Novak B., Housen B., Kitamura Y., Kanamatsu T. & Kawamura K. 2014: Magnetic fabric analyses as a method for determining sediment transport and deposition in deep sea sediments. *Mar. Geol.* 356, 19–30.

Olszewska B. & Wieczorek J. 1998: The Paleogene of the Podhale Basin (Polish Inner Carpathians) — micropaleontological perspective. *Przegl. Geol.* 46, 8/2, 721–728 (in Polish with English summary).

Ort M.H., Newkirk T.T., Vilas J.F. & Vazquez J.A. 2015: Towards the definition of AMS facies in the deposits of pyroclastic density currents. *Geol. Soc. London, Spec. Publ.* 396, 205–226.

Oszast J. & Stuchlik L. 1977: The Neogene vegetation of the Podhale (West Carpathians, Poland). *Acta Palaeobotanica* 18, 45–86 (in Polish with English summary).

Parés J.M. 2015: Sixty years of anisotropy of magnetic susceptibility in deformed sedimentary rocks. *Frontiers in Earth Science* 3, 4, 1–12.

Parés J.M., van der Pluijm B. A. & Dinarès-Turell J. 1999: Evolution of magnetic fabrics during incipient deformation of mudrocks (Pyrenees, northern Spain). *Tectonophysics* 307, 1–14.

Parés J. M., Hassold N. J. C., Rea D. K. & van der Pluijm B. A. 2007: Paleocurrent directions from paleomagnetic reorientation of magnetic fabrics in deep-sea sediments at the Antarctic Peninsula Pacific margin (ODP Sites 1095, 1101). *Ma. Geo.* 242, 4, 261–269.

Park C. K., Doh S. J., Suk D. W. & Kim K. H. 2000: Sedimentary fabric on deep-sea sediments from KODOS area in the eastern Pacific. *Mar. Geol.* 171, 1, 115–126.

Park M. E., Cho H., Son M. & Sohn Y. K. 2013: Depositional processes, paleoflow patterns, and evolution of a Miocene gravelly fan-delta system in SE Korea constrained by anisotropy of magnetic susceptibility analysis of interbedded mudrocks. *Mar. Petrol. Geol.* 48, 206–223.

Pešková I., Vojtko R., Starek D. & Sliva Ľ. 2009: Late Eocene to Quaternary deformation and stress field evolution of the Orava region (Western Carpathians). *Acta Geol. Pol.* 59, 1, 73–91.

Polášek S. 1959: Coal deposits of the Neogene Orava Basin. *Open file report*, *State Geol. Inst. of Dionýz Štúr*, Bratislava (in Slovak).

Pomianowski P. 2003: Tectonics of the Orava-Nowy Targ Basin — results of the combined analysis of the gravity and geoelectrical data. *Przegl. Geol.* 51, 6, 498–506 (in Polish with English summary).

Pospíšil L. 1990: The present possibilities of identification of shear zones in the area of the West Carpathians. *Mineralia Slovaca* 22, 19–31 (in Slovak with English summary).

Pulec M. 1976: Final report from the drillhole OH-1 (Hladovka — Orava Basin). *Open file report*, *State Geol. Inst. of Dionýz Štúr*, Bratislava (in Slovak).

R Core Team 2015: R: A language and environment for statistical computing. *R Foundation for Statistical Computing*, Vienna, Austria, www.r-project.org.

Rees A. I. 1961: The effect of water currents on the magnetic remanence and anisotropy of susceptibility of some sediments. *Geophys. J. Int.* 5, 3, 235–251.

Rees A. I. 1965: The Use of Anisotropy of Magnetic Susceptibility in the Estimation of Sedimentary Fabric. *Sedimentology* 4, 4, 257–271.

Rees A.I. & Woodall W.A. 1975: The magnetic fabric of some laboratory-deposited sediments. *Earth Planet. Sci. Lett.* 25, 2, 121–130.

Reinholdsson M., Snowball I., Zillén L., Lenz C. & Conley D. J. 2013: Magnetic enhancement of Baltic Sea sapropels by greigite magnetofossils. *Earth Planet. Sci. Lett.* 366, 137–150.

Roberts A. P., Chang L., Rowan C. J., Horng C. S. & Florindo F. 2011: Magnetic properties of sedimentary greigite (Fe_3S_4): An update. *Rev. Geophys.* 49, 1, 1–46.

Shimono T., Yamazaki T. & Inoue S. 2014: Influence of sampling on magnetic susceptibility anisotropy of soft sediments: comparison between gravity and piston cores. *Earth, Planets and Space* 66, 3, doi: 10.1186/1880-5981-66-3.

Shor A. N., Kent D. V. & Flood R. D. 1984: Contourite or turbidite?: Magnetic fabric of fine-grained Quaternary sediments, Nova Scotia continental rise. *Geol. Soc. London, Spec. Publ.* 15, 1, 257–273.

Sikora W. & Wieser T. 1974: Pyroclastic deposits in the Neogene of intramontane Orava-Nowy Targ Basin. *Geol. Quarterly* 18, 2, 441–443 (in Polish).

Soták J. 1998a: Sequence stratigraphy approach to the Central Carpathian Paleogene (Eastern Slovakia): eustasy and tectonics as controls of deep sea fan deposition. *Slovak Geol. Mag.* 4, 185–190.

Soták J. 1998b: Central Carpathian Paleogene and its constrains. *Slovak Geol. Mag.* 4, 203–211.

Struska M. 2008: Neogene-Quaternary structural development of the Orava Basin on the basis of geological, geomorphological and remote sensing investigations. *PhD thesis*, *AGH University of Science and Technology*, Cracow (in Polish).

Śmigielski M., Sinclair H.D., Stuart F.M., Persano C. & Krzywiec P. 2016: Exhumation history of the Tatry Mountains, Western Carpathians, constrained by low-temperature thermochronology. *Tectonics* 35, 1, 187–207.

Tamaki M., Suzuki K. & Fujii T. 2015: Paleocurrent analysis of Pleistocene turbidite sediments in the forearc basin inferred from anisotropy of magnetic susceptibility and paleomagnetic data at the gas hydrate production test site in the eastern Nankai Trough. *Mar. Petrol. Geol.* 66, 404–417.

Tarling D. H. & Hrouda F. 1993: The magnetic anisotropy of rocks. *Chapman & Hall*, London, 1–217.

Tokarski A.K. & Zuchiewicz W. 1998: Fractured clasts in the Domański Wierch series: Contribution to structural evolution of the Orava Basin (Carpathians, Poland) during Neogene through Quaternary times. *Przegl. Geol.* 46, 1, 62–66 (in Polish with English summary).

Tokarski A.K., Świerczewska A., Zuchiewicz W., Starek D. & Fodor L. 2012: Quaternary exhumation of the Carpathians: a record from the Orava-Nowy Targ Intramontane Basin, Western Carpathians (Poland and Slovakia). *Geol. Carpath.* 63, 257–266.

Tokarski A.K., Márton E., Świerczewska A., Fheed A., Zasadni J. & Kukulak J. 2016: Neotectonic rotations in the Orava-Nowy Targ Intramontane Basin (Western Carpathians): An integrated palaeomagnetic and fractured clasts study. *Tectonophysics* 685, 35–43.

Vass D., Kováč M., Konečný V. & Lexa J. 1988: Molasse basins and volcanic activity in West Carpathian Neogene–its evolution and geodynamic character. *Geol. Carpath.* 39, 539–562.

von Rad U. 1970: Comparison between "magnetic" and sedimentary fabric in graded and cross-laminated sand layers, southern California. *Geol. Rundsch.* 60, 1, 331–354.

Watycha L. 1971: Drillholes Czarny Dunajec IG-1 and Koniówka IG-1. *Open file report*, *Polish Geol. Inst.*, Warsaw (in Polish).

Watycha L. 1976a: The Neogene of the Orawa-Nowy Targ Basin. *Geol. Quarterly* 20, 3, 575–585 (in Polish with English summary).

Watycha L. 1976b: Detailed Geological Map of Poland 1:50,000. Sheet Czarny Dunajec (1048). *Polish Geol. Inst.*, Warsaw (in Polish).

Watycha L. 1977a: Explanations to the Detailed Geological Map of Poland 1:50,000. Sheet Czarny Dunajec (1048). *Polish Geol. Inst.*, Warsaw, 1–102 (in Polish).

Watycha L. 1977b: Explanations to the Detailed Geological Map of Poland 1:50,000. Sheet Jabłonka (1047). *Polish Geol. Inst.*, Warsaw, 1–72 (in Polish).

Watycha L. 1977c: Detailed Geological Map of Poland 1:50,000. Sheet Jabłonka (1047). *Polish Geol. Inst.*, Warsaw (in Polish).

Wetzel A. & Einsele G. 1991: On the physical weathering of various mudrocks. *Bulletin of the International Association of Engineering Geology* 44, 89–100.

Wiewióra A. & Wyrwicki R. 1980: Clay minerals of the Neogene sediments in the Orava-Nowy Targ basin. *Geol. Quarterly* 24, 2, 333–348 (in Polish with English summary).

Woźny E. 1976: Stratigraphy of the Younger Tertiary in the Orawa-Nowy Targ Basin on the basis of fresh-water and continental macrofauna. *Geol. Quarterly* 20, 3, 589–595 (in Polish with English summary).

Zachos J., Pagani M., Sloan L., Thomas E. & Billups K. 2001: Trends, Rhythms, and Aberrations in Global Climate 65 Ma to Present. *Science* 292, 686–693.

Zuchiewicz W., Tokarski A. K., Jarosiński M. & Márton E. 2002: Late Miocene to present day structural development of the Polish segment of the Outer Carpathians. *EGU Stephen Mueller Spec. Publ. Series* 3, 185–202.

Appendix

Dataset of all studied samples:

Sample name	# of spec.	GPS N 49°	GPS E 19°	Lithofacies code	AMS facies
Bo1	25	.46883	.71867	CL/Fm	Fm-unc
Bv1	25	.41923	.56145	Fm/Fl/CL	Fl
Bv2	25	.42451	.57049	Fmm	Fm-unc
Bv3	25	.41946	.56247	CL/Fm	Fm
By1	25	.39662	.88565	Sh	-
By2	25	.39819	.88749	Fm/Sm	Fm
By3	25	.39758	.88610	CL/Sm	-
CD1	25	.37584	.81073	Fm,Sh	Fm
CD2_1	25	.37717	.81087	Fm,Sm	Fm
CD2_2	24	.37717	.81087	CL,Fm	Hst
CD3_1	24	.38307	.80904	Hs	S
CD3_2	23	.38307	.80904	Hs	Hst
CD3_3	11	.38307	.80904	Hs	Hst
CD4	25	.38675	.80839	Fm	Fm
CD5	25	.39218	.81226	Sh	S
Ce1	18	.38256	.72894	Fm,CL	Fm
Ce3	25	.38294	.73601	Fm,CL	-
Ce4	25	.38470	.74141	CL,Fm	Fm
Ce5	25	.38468	.74194	Fm	Fm-def
Ce6	25	.38216	.73372	Fm	Fm-def
Ce7	25	.38340	.73830	Fm	Fm-def
Ce8	25	.38521	.74612	Fm,CL	Hst
Ce9	25	.38280	.73607	Fl,Hs	Hsl-def
Ce10	25	.38280	.73607	CL/Fl	Fl
Ce11	25	.38387	.74011	Fm,Sm	Fm-def
Ch1d	11	.43898	.64153	Fm	Fm
Ch1g	14	.43898	.64153	Fmm	S
Ch2	25	.42245	.67547	Fm	Fm
Ch3	25	.42924	.65929	Fm/Sm	S
Ch4	25	.41773	.70163	Sm,CL	Fm-unc
Chk1	25	.44452	.67485	Fmm	Fm-unc
CO1	25	.45813	.65983	Fm/Sm	Fm
DW1	25	.41326	.88376	Fm,CCL	CCL
Je1	13	.36620	.75947	Sh	S
Je2	10	.36620	.75947	Sh	S
Je3	10	.36620	.75947	CL	Hsl
Je4	14	.36659	.75791	CL/Fm	Fm
Je5	25	.40444	.67208	Fm	Fm
Je6	25	.38550	.72012	Fm/Sm	Fm
Je7	25	.38795	.71724	Fm/Sm	Fm
Je8	25	.39075	.71085	Fm	Fm
Je9	25	.36646	.75752	CL	Fl
Je10	25	.37799	.73299	Fm/CL	Fm-def

Sample name	# of spec.	GPS N 49°	GPS E 19°	Lithofacies code	AMS facies
JeQ1	25	.38313	.72669	Fm/Sm	Fm-unc
JeQ2	25	.38292	.73191	Fm/CL	Fm
JeQ3	25	.41092	.64495	Fm/Sm	Fm-unc
JeQ4	25	.40800	.66499	Sm/Fmm	S
JO1	25	.39997	.59163	Fm/Fl	Hsl
JO2	25	.40173	.59268	Sm/Fm	Fm
JO3	25	.41771	.59506	Fmc	Fm
JO4	25	.40431	.59484	Fm	Fm
JO5	25	.40431	.59484	Fm	Fm
JO6	25	.41076	.59050	Fl	Hsl
Ko1	10	.37320	.62711	CL	CLt-def
Ko2	25	.37324	.62712	CL	CLt-def
Koz1	25	.45038	.56984	Fm	Fm-unc
Krz1	25	.45337	.60597	CL	Fm-unc
Ku1	25	.45390	.67206	Fmm	Fm-unc
Li1	25	.46707	.64145	Sm	Fm
Li2	25	.47581	.63460	Fm/Sm	Fm
LM1	11	.48864	.65739	CCL,CL	CLt
LM2	25	.48842	.66577	Fm	Fm
Na1	25	.42027	.49771	Fm/CCL	Fm
OrCCL	25	.36638	.69957	CCL	CCL
OrCL	25	.36528	.70538	CL	CLt
OrCL_1	14	.36558	.70529	CL	Fl
OrCL2	25	.36638	.69957	CL	CLt
OrFl	25	.36542	.70542	Fl	Fl
OrFl2	25	.36560	.69844	Fl	Fl
OrFm	25	.36638	.69957	Fm	Fm
OrFm_3	9	.36575	.69759	Fm	Fm
OrFm_4	24	.36591	.69973	Fm	Fm
OrGmm	25	.36515	.70531	Gmm	-
OrHf_2	15	.36583	.70545	Hf	Fl
OrHs	24	.36560	.69844	Hs	Hsl
OrHs_3	13	.36575	.69759	Hs	Hsl
OrHs_5	23	.36576	.69949	Hs	Hst
OrSt	25	.36639	.70533	St	S
Tv1	25	.37539	.75807	Fm	Fm
Uh1	15	.37240	.63042	CL,Fm	Fm
UhQ2	25	.37235	.63242	Fmm	Fm
Us1	25	.38334	.57671	CL	CLt
Us2	25	.38351	.57823	Fm	Fm
Us3	25	.38434	.57971	CL,Fm	CLt-def
Wo1	25	.39956	.85846	Fm,CL	Fm-rot